recently reported by Avotina *et al.*[6] and with Grover's value of 37 h.[11] The only previously reported half-life determination with a mass-separated ^{147}Gd sample[12] yielded a value of 21.7±2.5 h, grossly at variance with our data.

In Table IV the energies of the most prominent γ rays associated with the decay of 38-h ^{147}Gd are listed, together with their abundances. The absolute abundances were calculated from the intensities of the 122- and 198-keV γ rays of ^{147}Eu that grew into the ^{147}Gd samples. For the number of 122- and 198-keV quanta per ^{147}Eu disintegration, the literature values[7] 0.20 and 0.24, respectively, were used. As can be seen in Table IV, the present values for the ^{147}Gd γ-ray energies and abundances are in fairly good agreement with those given by Avotina *et al.*[6]; however, these authors reported many additional γ rays which are either too low in intensity to have been seen in the present study or outside the energy range investigated.

[11] J. R. Grover, Phys. Rev. **126**, 1540 (1962).
[12] A. M. Friedman, J. Milsted, and O. Skilbreid, Phys. Rev. **129**, 1752 (1963).

ACKNOWLEDGMENTS

We wish to thank Dr. Erich Hechtl and Robert Zielinsky for assistance in some of the experiments. The invaluable cooperation and assistance of Dr. H. Bakhru during the Yale HILAC experiments is acknowledged with particular gratitude. Dr. Bruce Erdal kindly made his computer program for analysis of Ge(Li) γ spectra available.

PHYSICAL REVIEW VOLUME 187, NUMBER 4 20 NOVEMBER 1969

Transition Matrix Elements in the Even-Even Osmium Isotopes: A Comparison with Pairing-Plus-Quadrupole Model Calculations*

R. F. Casten,† J. S. Greenberg, S. H. Sie, G. A. Burginyon,‡ and D. A. Bromley

Wright Nuclear Structure Laboratory, Yale University, New Haven, Connecticut 06511

(Received 26 June 1969)

The energy-level structures and transition matrix elements between collective excitations in the even-even osmium isotopes ($A=186$–192) have been studied using Coulomb excitation with oxygen projectiles having incident energies between 42 and 80 MeV. The deexcitation γ radiations have been observed with NaI(Tl) and Ge(Li) detectors, singly, in coincidence with inelastically backscattered O^{16} ions, and in coincidence with γ rays from the $2^+\rightarrow 0^+$ and $4^+\rightarrow 2^+$ transitions in each isotope. Angular-correlation studies have been performed on all observed transitions following Coulomb excitation by backscattered ions. In the four isotopes studied, all levels through the 6^+ state of the ground-state band as well as the second excited $2^{+\prime}$ and $4^{+\prime}$ states have been populated, and the transition moments associated with the excitation of these states have been measured. In Os^{192}, previously unobserved radiations have been assigned to the deexcitation of a 6^+ state at 1088 keV and a $4^{+\prime}$ state at 907 keV. Except for the observation of the 0^+ state at 1086 keV in Os^{188}, a search for low-lying 0^+ states in the other osmium isotopes did not reveal any definite candidates. Electric-quadrupole transition matrix elements have been deduced from the data with a model-independent analysis using the Winther–de Boer computer code for multiple Coulomb excitation. The latter quantities, together with measured branching ratios and $B(M1)$ values, have been compared with several macroscopic and microscopic nuclear models, with particular attention to the pairing-plus-quadrupole model of Kumar and Baranger. The latter has proved to be the most complete and successful of the models tested in predicting both absolute $B(E2)$ values, and the variation of these with neutron number in the osmium isotopes. However, the model in its original form makes the transition from deformed to spherical shape more rapidly, with increasing mass, than appears to be the case experimentally, thereby suggesting the need for small variations in the relative strength of the pairing and quadrupole nucleon-nucleon residual forces assumed as input to the microscopic calculations. A description of the osmium isotopes, as typified by shallow potential minima for moderately prolate deformations (in the cases of $Os^{190,192}$ asymmetric equilibrium configurations) and by pronounced softness to both β and γ vibrations, emerges from the comparisons made.

I. INTRODUCTION

In the evaluation of the significance of various theories of nuclear collective motion, the study of the transitional nuclei at the upper and lower mass limits of the rare earths has been very useful. In particular, a description, on both the microscopic and phenomonological levels, of the evolution from the harmoniclike structure of the "vibrator" nuclei to the rotational-like structure of nearby nuclei with large static quadrupole deformations has been sought in recent investigations. It is evident from the existing data that as one moves away from those few nuclei for which the rotational and vibrational limits are good

* Work supported by the U. S. Atomic Energy Commission under Contract No. AT(30-1)3223.
† Present address: Niels Bohr Institute, Copenhagen, Denmark.
‡ Present address: Lawrence Radiation Laboratory, Livermore, Calif.

approximations, the agreement between the theoretical predictions based on perturbation methods to treat the departures from these limits and the experimental data rapidly deteriorates. In fact, calculations based on a pure vibrational model have enjoyed few and limited successes; the discovery of large static quadrupole moments for excited states of nuclei heretofore considered nearly spherical in their ground states have amplified the shortcomings of this point of view, and have indicated that even for these nuclei, a large departure from harmonicity is evident with large fluctuations about the equilibrium shape in the excited states.[1] In nuclei which exhibit principally a rotational structure, such as is characteristic of some of the Sm and Gd isotopes, the perturbation treatments of the coupling of rotations with the β and γ vibrations have not been adequate to reproduce the available data on transition rates and on excitation spectra, and inconsistencies remain unexplained.

All these phenomena are brought into sharp focus to varying degrees in the transition nuclei. Here, we report on an investigation on nuclei near the high-mass transitional region of the rare earths, the even-even isotopes of osmium ($Os^{186,188,190,192}$), in which Coulomb excitation by O^{16} ions was used to populate the low-lying excited states and permit measurement of the reduced transition probabilities between these states. The latter are an important check on calculations, since they constitute a sensitive test of the detailed model wave functions. The even-even osmium isotopes are of particular interest, since their level structure exhibits a relatively slow transition from a harmonic pattern at the high-mass end to a rotational structure at the low-mass end, so that the effects mentioned above may be studied under slowly varying conditions.[2] (This is in striking contrast to the much more abrupt transition which occurs at the lower end of the rare-earth region of deformation; e.g., between Sm^{150} and Sm^{152}). In addition, this particular group of nuclei has recently taken on increased interest reflecting the encouraging initial successes of calculations performed by Kumar and Baranger in this mass region.[3]

These calculations are free of many of the limiting assumptions mentioned above. A microscopic pairing-plus-quadrupole residual interaction between independent spherical-shell-model states is used to evaluate the seven inertial functions which enter the Bohr Hamiltonian, and the Schrödinger equation is solved exactly numerically; the strength of the pairing force is determined by fitting the odd-even mass differences for the entire region $Z=50$–82, and $N=89$–126; the strength of the quadrupole forces and the effective charge are obtained from the experimental intrinsic quadrupole moments over the same mass region with an adjustment of at most a few percent allowed from nucleus to nucleus to fit the data. The solution for the eigenfunctions and eigenvalues, as a function of the collective coordinates β and γ, makes no assumption of small oscillations in β and γ or of separability of rotations and of β and γ vibrations. Although the residual interactions used may not be realistic, these calculations at least form a starting point for further work.

The model has been applied to the Os, W, and Pt nuclei with considerable success.[3] Predicted energy levels, magnetic moments of the first 2^+ states, and $B(E2; 0^+ \rightarrow 2^+)$ values are in reasonable agreement with experiment. Furthermore, the model is the first which successfully predicts finite excited-state static quadrupole moments in nuclei where the ground state has been previously assumed to be spherical. It is evident that these successful aspects of the calculations encourage more demanding comparisons and further detailed tests of the model wavefunctions. Such tests are partially provided by the measurement of the transition probabilities between states, particularly at high excitation energies.

Data concerning the low-energy excitations of the osmium isotopes have been accumulated including energy levels, spins, parities, multipole mixing ratios, and some branching ratios for decay of excited states.[2,4–24] Except for this and concurrent work,[25] $B(E2)$ measurements have been limited to those transi-

[1] J. deBoer and J. Eichler, in *Advances in Nuclear Physics*, edited by M. Baranger and E. Vogt (Plenum Press, Inc., New York, 1968), Vol. 1.

[2] G. T. Emery, W. R. Kane, M. McKeown, M. L. Perlman, and G. Sharff-Goldhaber, Phys. Rev. **129**, 2597 (1963); G. Sharff-Goldhaber, in *Proceedings of the University of Pittsburgh Conference on Nuclear Structure, 1957* (University of Pittsburgh and Office of Ordnance Research, U. S. Army, 1957).

[3] K. Kumar and M. Baranger, Nucl. Phys. **92**, 608 (1967); M. Baranger and K. Kumar, *ibid.* **A110**, 490 (1968); K. Kumar and M. Baranger, *ibid.* **A110**, 529 (1968); M. Baranger and K. Kumar, *ibid.* **A122**, 241 (1968); K. Kumar and M. Baranger, *ibid.* **A122**, 273 (1968).

[4] B. Harmatz and T. H. Handley, Nucl. Phys. **56**, 1 (1964).

[5] F. R. Metzger and R. D. Hill, Phys. Rev. **82**, 646 (1951).

[6] W. I. King and M. W. Johns, Can. J. Phys. **37**, 755 (1959).

[7] M. L. Lark and H. Morinaga, Nucl. Phys. **63**, 466 (1965).

[8] J. O. Newton, F. S. Stephens, and R. M. Diamond, Nucl. Phys. **A95**, 377 (1967).

[9] M. Sakai *et al.*, Nucl. Phys. **74**, 81 (1965).

[10] H. Ejiri *et al.*, J. Phys. Soc. Japan **21**, 1021 (1966).

[11] T. Yamazaki and D. L. Hendrie, in *Proceedings of the International Conference on Nuclear Physics*, Gatlinburg, Tenn., 1966 (Academic Press Inc., New York, 1967).

[12] J. Burde, R. M. Diamond, and F. S. Stephens, Nucl. Phys. **A92**, 306 (1967).

[13] R. E. Arns, R. D. Biggs, and M. L. Wiedenbeck, Nucl. Phys. **15**, 125 (1960).

[14] I. Markland, B. von Nooijen, and Z. Grabowski, Nucl. Phys. **15**, 533 (1960).

[15] O. B. Nielsen, N. O. Roy Poulsen, R. K. Sheline, and B. Skytte Jensen, Nucl. Phys. **10**, 475 (1959).

[16] E. Bashandy and S. G. Hanna, Nucl. Phys. **84**, 577 (1966).

[17] T. Yamazaki, Nucl. Phys. **44**, 353 (1963).

[18] W. R. Kane, thesis, Harvard University, 1959 (unpublished).

[19] L. B. Warner and R. K. Sheline, Nucl. Phys. **36**, 207 (1962).

[20] H. Ikegami, T. Hirose, M. Sakai, T. Yamazaki, and K. Sugiyama, J. Phys. Soc. Japan Suppl. **24**, 167 (1968).

[21] W. R. Kane, G. T. Emery, G. Scharff-Goldhaber, and M. McKeon, Phys. Rev. **119**, 1953 (1960).

[22] J. Blachot, E. Monnand, and A. Moussa, Compt. Rend. **261**, 1835 (1965).

[23] L. L. Baggerly, P. Meunier, F. Boehm, and J. S. Dumond, Phys. Rev. **100**, 1364 (1955).

[24] D. K. Butt and B. C. Dutta, Nucl. Phys. **39**, 517 (1962).

[25] W. T. Milner, F. K. McGowan, R. L. Robinson, and P. H. Stelson, Bull. Am. Phys. Soc. **12**, 35 (1967); W. T. Milner, thesis, University of Tennessee, 1968 (unpublished).

tions involving the ground state and the lowest three excited states in $Os^{188,192}$, the lowest two 2^+ states in Os^{190}, and the first 2^+ state in Os^{186}.[26–35] However, except for the $B(E2; 0^+ \rightarrow 2^+)$ values from lifetime and Coulomb excitation measurements, the $B(E2)$ values were generally known with poor accuracy (30–40%), with frequent large disagreement among different observers. In the present experiments the high excitation probabilities induced by O^{16} ions, with energies up to 80 MeV, were used to extend the existing information on transition probabilities to higher-spin states, as well as to provide further accurate measurements on the lower-lying states. $B(E2)$ values and branching ratios relating to the lowest three excited states were obtained for the four nuclei, $Os^{186,188,190,192}$. Higher-lying 6^+, $4^{+\prime}$, $0^{+\prime}$, and other previously unobserved states were also populated, and in most cases $B(E2)$ values for the excitation of these states were evaluated. (A prime on a state label will be used to indicate the second occurrence of a state of that J^π in a given nucleus). Some of the results reported here, including partial comparisons of the predictions of Kumar and Baranger[3] with our experimental results, have previously been communicated.[36] These results have been updated to include new measurements in addition to the preliminary measurements on which the earlier communications were based. The new and more comprehensive data have resulted in some modification of the earlier results. Concurrent and overlapping investigations have been performed by Milner *et al.*,[25] using protons, α particles, and O^{16} ions with energies up to 49 MeV.

II. EXPERIMENTAL PROCEDURES

O^{16} ion beams of 42.00, 48.26, 62.00, 70.01, 70.30, and 80.00 MeV obtained from the Yale MP Tandem Van de Graaff accelerator were used to bombard both thick and thin self-supporting isotopically enriched targets of the four even-even osmium isotopes. Deexcitation γ radiation was observed with both the Ge(Li) and the NaI(Tl) detectors. Coincidence experiments were performed between γ rays and backscattered ions, and between γ rays from the transitions $2^+ \rightarrow 0^+$ and $4^+ \rightarrow 2^+$ in the ground-state band and γ rays feeding the 2^+ and 4^+ states. γ-ray angular distribution measurements were carried out in all cases for both the measurements involving the detection of the γ rays singly and for those in which the γ rays were detected in coincidence with backscattered ions.

The bulk of the data at all the bombarding energies were accumulated using a NaI(Tl) detector. Simultaneous with these measurements, deexcitation γ radiation was observed with a Ge(Li) detector. Complete, and separate, coincidence experiments were also carried out at a bombarding energy of 70.01 MeV with the Ge(Li) detector, including measurements of the γ-ray angular distributions. The latter data were particularly significant in establishing the γ-ray transitions from the higher excited states populated.

The reduced transition probabilities were calculated using almost exclusively the γ-backscattered-ion coincidence data. This approach was adopted because of the significant simplification which it affords in the data analysis, in addition to the often discussed advantages of reliable normalization, reduction of backgrounds due to low Z target contaminants, and enhanced probabilities in the excitation of the higher excited states because of the correspondence between the backscattered ions and the closer distances of approach of the exciting ions to the nuclear surface. The simplification in the analysis arises from the consideration that for zero-spin projectiles and target nuclei, and for scattering angles near 180°, the contribution to the excitation from magnetic substates other than $M=0$ is necessarily small. The most forward center-of-mass scattering angle in these measurements was about 158°; in this case the neglect of all contributions except from the $M=0$ state leads to uncertainties in the integrated yields of less than 1.5% for excitation of any state observed in this experiment and, generally, to substantially lower uncertainties. This circumstance is particularly useful for high-energy projectiles, with which many nuclear levels can be excited, and a complete analysis requires the solution of the coupled Schrödinger equations for the excitation amplitudes. The $M=0$ approximation reduces by factors of 3 or more the number of such equations to be solved. Furthermore, this approximation renders the γ-ray angular distribution independent of the incident projectile energy and of the excitation route, greatly simplifying the application of an angular distribution correction to the data.

A. Apparatus

The experimental arrangement used in the thin-target experiments is indicated in Fig. 1. The scattering chamber employed for the experiments with thick targets was identical to the chamber shown in Fig. 1, except that it terminated at the neck of the horn-shaped

[26] D. H. Rester, M. S. Moore, F. E. Durham, and C. M. Class, Nucl. Phys. **27**, 104 (1961).
[27] F. K. McGowan, Phys. Rev. **81**, 1066 (1951).
[28] E. E. Berlovich, Zh. Eksperim. i Teor. Fiz. **33**, 1522 (1957) [English transl.: Soviet Phys.—JETP **6**, 1176 (1958)].
[29] D. B. Fosson and B. Herskind, Nucl. Phys. **40**, 24 (1963).
[30] E. Bashandy and El-nesr, Nucl. Phys. **34**, 483 (1962).
[31] J. de Boer, G. Goldring, and H. Winkler, Phys. Rev. **134**, B1032 (1964).
[32] F. K. McGowan and P. H. Stelson, Phys. Rev. **122**, 1274 (1961).
[33] F. K. McGowan and P. H. Stelson, Phys. Rev. **109**, 901 (1958).
[34] R. Barloutaud, P. Lehman, and A. Leveque, Compt. Rend. **245**, 523 (1957).
[35] A. W. Sunyar, in *Proceedings of the Second United Nations International Conference on the Peaceful Uses of Atomic Energy, Geneva, 1958* (United Nations, Geneva, 1958).
[36] R. F. Casten, J. S. Greenberg, G. A. Burginyon, D. A. Bromley, and G. Holland, Bull. Am. Phys. Soc. **12**, 35 (1967); R. F. Casten, J. S. Greenberg, G. A. Burginyon, and D. A. Bromley, Phys. Rev. Letters **18**, 912 (1967).

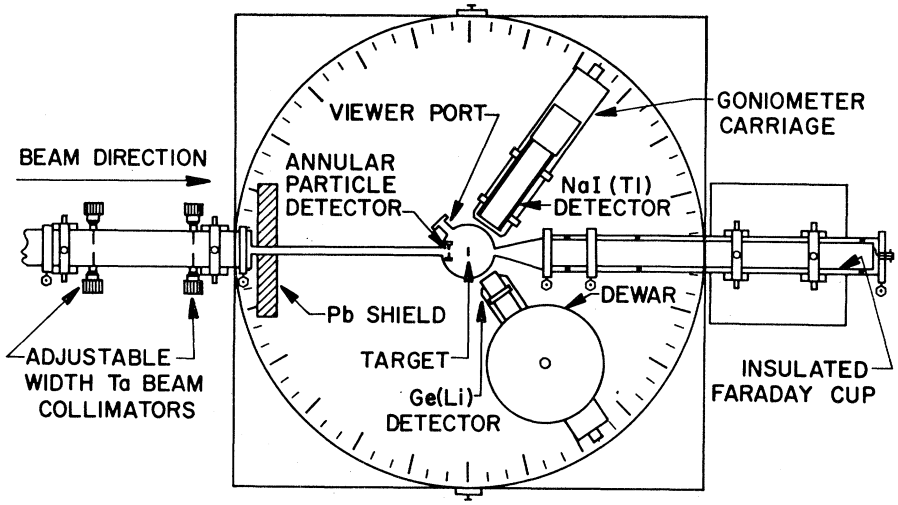

FIG. 1. Plan view of scattering chamber and apparatus used for the measurements with thin targets. A modified scattering chamber was used for the experiments employing thick targets that terminated at the neck leading to the Faraday cup. During the γ-γ coincidence measurements, a 3×3-in. NaI(Tl) detector was placed in the position occupied by the Ge(Li) detector in the diagram.

beam tube leading to the Faraday cup. For the latter arrangement, the beam was stopped in the thick targets, and the whole forward hemisphere was accessible to the γ-ray detector, including 0°. During the γ-γ coincidence studies, a second Na(Tl) detector occupied the position of the Ge(Li) detector shown in Fig. 1. To accommodate the lower intrinsic efficiency and smaller dimensions of the Ge(Li) detector, a third scattering chamber was used for the coincidence studies with the Ge(Li) detector. With this chamber, the distance between the target and the γ-ray detector could be reduced considerably over the closest distance accessible with the chamber shown in Fig. 1.

The incident beam was collimated by two adjustable rectangular apertures sufficiently upstream from the scattering chamber so that the background contribution from slit scattering was negligible. Four or more targets could be inserted simultaneously in the scattering chamber and any part of each could be exposed to the incident beam with controls outside the chamber.

An annular silicon surface-barrier particle detector was used in the γ-particle coincidence measurements. It was centered along the beam axis and subtended a laboratory angle of 14° between 158° and 172°. Typically, the depletion depth of the counter was chosen to stop 80-MeV O^{16} ions. In the measurements employing thick targets, the effective target thickness used in the thick-target integrations was specified by an electronic threshold on the particle-detector pulse output corresponding to a particle energy $E=E_m$ below which no γ-particle coincidences were recorded. This cutoff energy was chosen empirically, on the basis of previous studies, to exclude particles originating from interactions with low Z contaminants in the target. The thin-target-particle spectra showed a very well defined peak, in which the elastic scattering and the inelastic scattering corresponding to Coulomb excitation were unresolved. The cutoff energy for the particle counter in the latter cases was chosen to include the excitation of all the states of interest. The background contribution to the γ-particle coincidence rate from reactions with the low Z target contaminants was completely negligible. The 3×3 in. NaI(Tl) γ-ray detector was located 6.5 cm from the target, and in most of the measurements at 55° to the incident beam direction. In the γ-γ coincidence studies, the second NaI(Tl) detector was set in a conjugate position. Two Ge(Li) detectors of 7 and 22 cm^3 were used. The γ-ray counters were mounted on independently moveable radial arms, and the attainable precision for the angle determination was $\pm 0.2°$. The degree of alignment between the axis of rotation for the γ-ray detectors, and the point of intersection of the beam and target, was measured by placing a radioactive source at the latter position and studying the deviations from the expected isotropy in the angular distribution. An in-beam study was also performed by measuring the ratio of counting rates at conjugate angle positions.

Graded absorbers were employed to reduce pile-up effects from γ-ray transitions deexciting the strongly populated first excited states. Energy calibrations for the γ-ray detectors were performed with standard sources and supplemented by internal calibrations employing the previously well-established transitions in the nuclei studied. Standard spectral shapes and efficiency calibrations were obtained with monoenergetic calibrated sources in the counter geometries and with the absorber conditions employed in the experiment. The accuracy with which the absolute efficiencies of the γ-ray detectors is known, including uncertainties in the absorption corrections, is estimated to be $\pm 5\%$ for all transitions except the $2^+ \rightarrow 0^+$ deexcitations. The

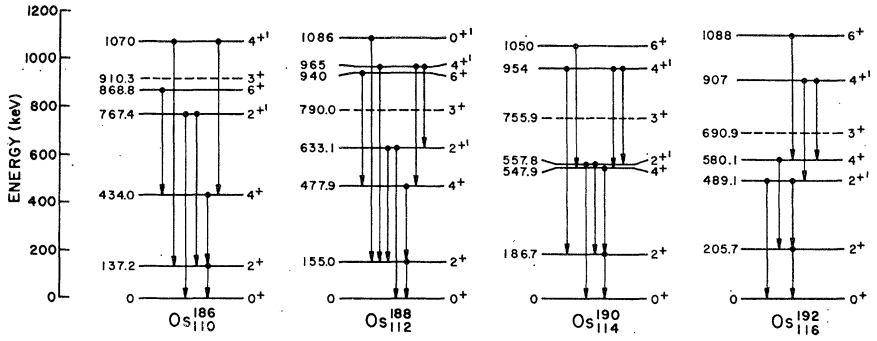

FIG. 2. Partial energy-level diagrams for $Os^{186,188,190,192}$. The arrows indicate transitions observed in these measurements following Coulomb excitation with O^{16} ions. The values for the energies given in the figure were taken from Refs. 2 and 4, and from our measurements.

uncertainty in the relative peak efficiencies for the Ge(Li) detector is estimated to be $\pm 2.5\%$ for γ-ray energies between 200 keV and 1.5 MeV. For the $2^+ \rightarrow 0^+$ transitions, absorption corrections for the measurements involving thick targets are relatively large. Because of uncertainties regarding the uniformity of the thick targets, an additional error of up to $\pm 10\%$ must be ascribed to the efficiency determination in the thick-target measurement for the $2^+ \rightarrow 0^+$ transitions. For the experiments involving thin targets, the error contribution due to target absorption is negligible.

B. Targets

As noted above, both thick and thin targets were used. The average thickness for the former was 0.003 in., while the latter were in the range 500–1000 $\mu g/cm^2$. All targets were self-supporting and isotopically enriched. Virtually all contaminants in each case were the other osmium isotopes. The thick targets were fabricated by shaping the metallic osmium powder into disk form and mechanically pressing it between two slabs of carborundum. The sintered disks resulting from this procedure were annealed by electron bombardment under vacuum. The thin targets were fabricated by evaporation from a tungsten boat onto a glass substrate using electron bombardment for heating. Subsequent water floatation of the evaporated films allowed them to be picked up on tantalum target supports. Details regarding the fabrication procedures will be published elsewhere.

III. RESULTS

A. Excitation Spectra

The low-energy spectra of the even osmium isotopes have been investigated extensively through study of the radioactive decay of neighboring nuclei and in $(\alpha, 2n)$ and $(p, 2n)$ reactions. Decay-scheme information obtained from this investigation is, therefore, largely of a corroborative nature, apart from the establishment of a number of new transitions. A number of the previously known, higher-lying states have been Coulomb excited for the first time. All the data presented herein are untreated insofar as no corrections have been made for contaminants in the targets. In the Os^{186} target, the 61.5% isotopic enrichment was insufficient to preclude observation of strong transitions from the other Os isotopes; for analysis purposes, those transitions were subtracted from the spectra using equivalent data taken under identical conditions for the contaminant isotopes. In all the particle coincidence spectra, subtraction of accidental coincidences contributes to no more than a 2% correction in the NaI(Tl) data, and approximately 10% in the Ge(Li) data.

Each spectrum is dominated by four strong transitions originating from the excitation of the first 2^+ and 4^+ states in the ground-state band, and the $2^{+\prime}$ state in the γ band. (The band nomenclature is used here, in the usual sense, for identification purposes only and does not imply the correctness of the model.) Present at reduced intensities in all isotopes are transitions from the 6^+ member of the ground-state band and from the $4^{+\prime}$ member of the γ band. At least two branchings, and sometimes three branchings, are observed in the deexcitation of the $4^{+\prime}$ states which allows the determination of the intraband and interband-intraband branching ratios for the $4^{+\prime}$ states. From the latter ratios, the ratios of the transition moments $|Q_{22}|/|Q_{00}|$, $|Q_{20}|/|Q_{00}|$, and $|Q_{20}|/|Q_{22}|$, defined in Sec. VI, have been extracted. The theoretically important ratio $B(E2; 2^{+\prime} \rightarrow 2^+)/B(E2; 2^{+\prime} \rightarrow 0^+)$ has been determined from the deexcitation of the strongly excited $2^{+\prime}$ state.

Partial level diagrams for the four Os isotopes studied are shown in Fig. 2, including all the levels and transitions observed in these experiments to which definite spins and parities may be assigned. In addition, the 3^+ levels are shown for continuity although, being of unnatural parity, they are only very weakly excited in Coulomb excitation. The multipolarity of the transitions and their generic origin are independently obtained, in this experiment, from angular distribution studies of the γ radiations, excitation function measurements, and γ-γ coincidence measurements of which details are discussed in subsequent sections.

The systematics of the Os transition region are clear from this figure. Proceeding toward Os^{192}, the ground-state rotational band energies increase monotonically as the moments of inertia and deformations decrease. The $2^{+\prime}$, 3^+, and $4^{+\prime}$ levels, on the other hand, decrease

in energy as the nuclei tend towards γ instability or at least towards axially asymmetric equilibrium shapes. More quantitatively, the energy ratio, E_{4^+}/E_{2^+}, varies from 3.17 (close to the rotational limit, 3.33) in Os^{186} to a value of 2.82 in Os^{192}, much closer to the ratio 2.2 often found in so-called "vibrational" nuclei. Furthermore, the results of the next section show that the ratio $B(E2; 2^{+\prime}\rightarrow 2^+)/B(E2; 2^{+\prime}\rightarrow 0^+)$ varies from 2.2 in Os^{186} to 8.4 in Os^{192}. The rotational model values for this ratio is 1.43, whereas it is infinite within the framework of the simple vibrational model.

Although spectra are shown here for only one bombarding energy, all isotopes were studied at the six bombarding energies mentioned above. Below, we outline briefly some of the features of the γ-ray spectra which are relevant to the subsequent discussion.

1. Os^{186} Nucleus

Because the other three stable even Os nuclei occur in significant isotopic abundances in the target used, the γ-ray spectra for the Os^{186} target contain strong contributions from all four Os isotopes. The near degeneracy in some of these transitions emphasizes the importance of the Ge(Li) data in the analysis of these spectra. An example of Ge(Li) singles and γ-particle coincidence spectra at a bombarding energy of 70.01 MeV is shown in Fig. 3. The NaI(Tl) spectra are not shown in this case, since they add no further information beyond verification in the γ-γ coincidence data of the origin of the 434.8-, 630.2-, and 933-keV transitions. The contaminant γ rays are indicated in the figure. The three strong transitions at 137.2, 296.8, and 434.8 keV in the γ-particle spectrum originate from the well-established 2^+, 4^+, and 6^+ levels at 137.2, 434.0, and 868.8 keV. The cascade nature of these γ rays was established in the γ-γ coincidence measurements, and the multipolarities of the transitions, discussed in Sec. III-B, were verified in the γ-particle coincidence angular distribution measurements and in the variation of the yield of γ rays with bombarding O^{16} ion energy. The usual enhancement in the population of the higher-spin states, when large angle scatterings for the O^{16} ion are selected, is evident. No clear evidence was found for the excitation of the 8^+ state, although statistically significant peaks occur at energies near 584 and 552 keV where contradictory assignments[2,8,10] have been made for the $8^+\rightarrow 6^+$ transition. Because of resolution limitations, and the level of background radiation, the γ-γ coincidence data do not distinguish between these two choices.

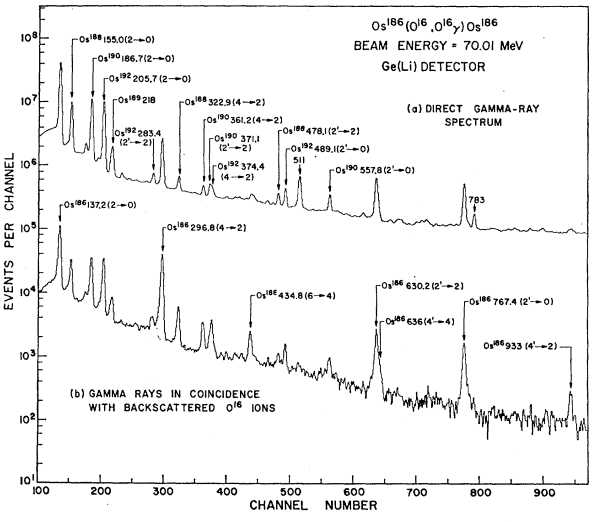

FIG. 3. γ-ray spectra obtained with a 22-cm² Ge(Li) detector following Coulomb excitation of 61.5% enriched Os^{186} with 70.01-MeV O^{16} ions: (a) direct singles spectrum; (b) spectrum taken in coincidence with backscattered O^{16} ions. The energy of the γ rays is given in keV. The spin change associated with each γ ray transition is indicated in the figure. Some of the prominent transitions not originating from Coulomb excitation of Os^{186} have been identified in the figure.

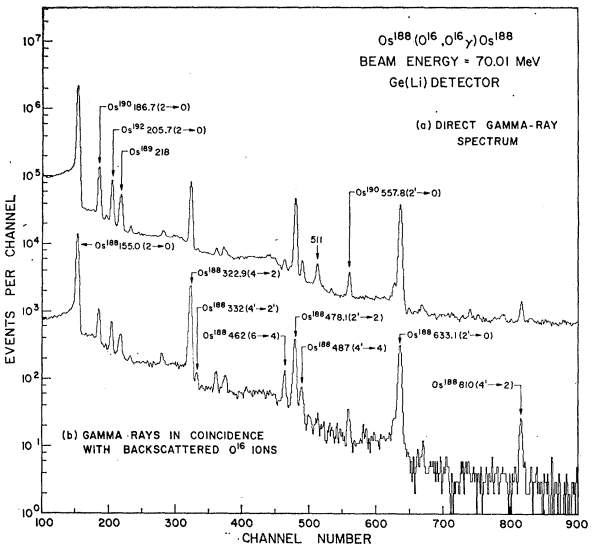

FIG. 4. γ-ray spectra obtained with a 22-cm² Ge(Li) detector following Coulomb excitation of 87.7% enriched Os^{188} with 70.01-MeV O^{16} ions: (a) direct singles spectrum; (b) spectrum taken in coincidence with backscattered O^{16} ions. The energy of the γ rays is given in keV. The spin change associated with each γ-ray transition is indicated in the figure. Some of the prominent transitions not originating from Coulomb excitation of Os^{188} have been identified in the figure.

The peak near 630 keV in the γ-particle coincidence spectrum is noticeably broader than the instrumental width near this energy. It consists principally of the 630.2-keV ($2^{+\prime}\rightarrow 2^+$) transition in Os^{186} with contributions from the 633.1-keV ($2^{+\prime}\rightarrow 0^+$) transition in Os^{188} and the 636-keV ($4^{+\prime}\rightarrow 4^+$) transition in Os^{186}. The fraction reflecting the 633.1-keV transition was subtracted by normalization to the yield of the prominent transitions at 155.0, 322.9, and 478.1 keV in the Os^{188} spectra taken under identical conditions. The relative intensities of the 630.2- and 636-keV peaks were then determined by fitting this composite peak with standard peak profiles at these energies. The intensity ratio

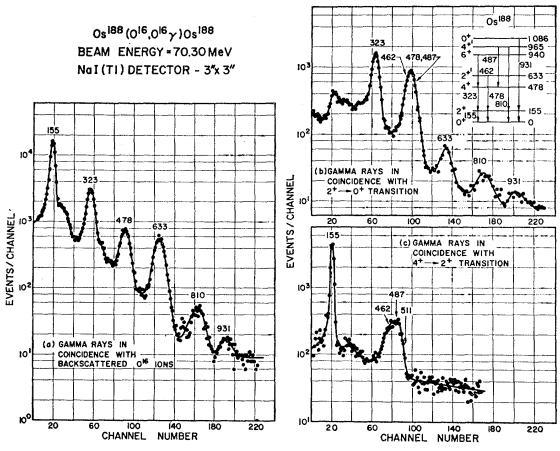

FIG. 5. NaI(Tl) γ-ray spectra following Coulomb excitation of 87.7% enriched Os^{188} with 70.30-MeV O^{16} ions: (a) spectrum taken in coincidence with backscattered O^{16} ions; (b) and (c) spectra taken in coincidence with the 155-keV $(2^+ \rightarrow 0^+)$ and 323-keV $(4^+ \rightarrow 2^+)$ transitions in the ground-state band of Os^{188}.

$I(4^{+\prime} \rightarrow 4^+)/I(4^{+\prime} \rightarrow 2^+) = 1.85 \pm 0.46$ thus evaluated, agrees with the values previously reported.[2,4] Another check on this procedure is available from the singles data where the contribution of the $(4^{+\prime} \rightarrow 4^+)$ transition to the 630.2 keV is small and resolved from the 636-keV line once the 633.1-keV contribution has been subtracted. The contribution of the $(2^{+\prime} \rightarrow 0^+)Os^{188}$ transition is removed here with the procedure used in the coincidence spectrum. The value for the intensity ratio $I(2^{+\prime} \rightarrow 2^+)/I(2^{+\prime} \rightarrow 0^+)$ evaluated from the singles data agrees well within the measurement errors with the value obtained from the coincidence data.

2. Os^{188} Nucleus

As in the case of the Os^{186} nucleus, the lowest excitation spectra in Os^{188} again may be grouped into two rotational bands based, respectively, on the ground state and the second excited 2^+ level. Ge(Li) singles and particle-γ coincidences spectra recorded for Os^{188} are shown in Fig. 4, while sample γ-γ and γ-particle spectra, taken with NaI(Tl) detectors, are illustrated in Fig. 5. The four principal peaks at energies of 155.0, 322.9, 478.1, and 633.1 keV correspond predominately to the $2^+ \rightarrow 0^+$, $4^+ \rightarrow 2^+$, $2^{+\prime} \rightarrow 2^+$, and $2^{+\prime} \rightarrow 0^+$ deexcitations, respectively, although in the NaI(Tl) spectra, the last two peaks have additional contributions from other transitions. Weaker peaks at 332, 462, 487, 810, and 931 keV originate from deexcitation of levels not previously Coulomb excited.

The γ rays at 332, 487, and 810 keV, seen clearly in the Ge(Li) γ-particle coincidence spectrum, represent the $4^{+\prime} \rightarrow 2^{+\prime}$, $4^{+\prime} \rightarrow 4^+$, and $4^{+\prime} \rightarrow 2^+$ transitions. The 810-keV transition is in coincidence (Fig. 5) with the $2^+ \rightarrow 0^+$ γ ray, but is not in coincidence with the $4^+ \rightarrow 2^+$ transition. All three γ rays, when taken in coincidence with backscattered particles, have the required angular distribution for the spin changes indicated and for $E2$ multipolarity. In addition, these assignments result in the satisfactory reproduction of the population of the $4^{+\prime}$ state with incident O^{16} ion energy. The 931-keV transition shown in Fig. 5 would be expected from the $0^{+\prime} \rightarrow 2^+$ deexcitation in this nucleus. That it is in coincidence with the $2^+ \rightarrow 0^+$ transition (Fig. 5), but not with the $4^+ \rightarrow 2^+$ deexcitation, provides further support for this interpretation. Once again, the energy dependence of the population of this state and the angular distribution from the γ-particle data provides supportive evidence.

The 462-keV $(6^+ \rightarrow 4^+)$ transition cannot be resolved in the NaI(Tl) spectra, from the intense $2^{+\prime} \rightarrow 2^+$ and the weak $4^{+\prime} \rightarrow 4$ transitions. Coincidences taken with γ rays from the 4^+ state indicate a broad peak which may be decomposed into the 462-keV $(6^+ \rightarrow 4^+)$, and 487-keV $(4^{+\prime} \rightarrow 4^+)$ peaks, showing that both these transitions terminate on a level in the ground-state band of spin 4^+ or higher. In the Ge(Li) data, where all three peaks are well resolved, the $6^+ \rightarrow 4^+$ transition has the expected enhancement when the singles and γ-particle data are compared; in addition it exhibits the expected angular distribution for a $6^+ \rightarrow 4^+$ transition discussed in Sec. V. The energy measured for the $6^+ \rightarrow 4^+$ transition is in agreement with the value quoted in Ref. 8, but in disagreement with the transition energy determined in Ref. 7, the latter having been obtained under more difficult experimental conditions.

In the NaI spectra, the decomposition of the composite peak consisting of the $2^{+\prime} \rightarrow 2^+$, $6^+ \rightarrow 4^+$, and $4^{+\prime} \rightarrow 4^+$ transitions was achieved through use of the measured branching ratios for the $4^{+\prime}$ state together with the intensity of the resolved $4^{+\prime} \rightarrow 2^+$ 810-keV transition, as well as the distinct variation with incident O^{16} energy, of the observed branching ratio of the $2^{+\prime}$ state. If the

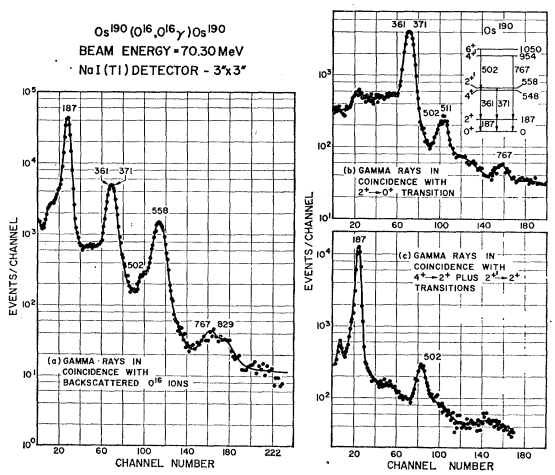

FIG. 6. NaI(Tl) γ-ray spectra obtained following Coulomb excitation of 95.46% enriched Os^{190}: (a) spectrum taken in coincidence with backscattered O^{16} ions; (b) and (c) spectra taken in coincidence with the 187-keV $(2^+ \rightarrow 0^+)$ and 361-keV $(4^+ \rightarrow 2^+)$ transitions in the ground-state band of Os^{190}.

total intensity of the peak near 478 keV is assigned to the $2^{+\prime}\rightarrow 2^{+}$ γ ray, it is found that the $(2^{+\prime}\rightarrow 2^{+})/(2^{+\prime}\rightarrow 0^{+})$ branching ratio varies with bombarding energy. This variation is attributable to the contributions from the excitation of the 6^{+} and $4^{+\prime}$ states. As the incident O^{16} energy is increased, the $(2^{+\prime}\rightarrow 2^{+})/(2^{+\prime}\rightarrow 0^{+})$ ratio increases owing to the additional transitions from the higher spin states. The energy dependence of the excitation of the circuitously populated 6^{+} and $4^{+\prime}$ states is much stronger than that of the $2^{+\prime}$ state; consequently, the $2^{+\prime}$ state deexcitation branching ratio varies by more than 30% as O^{16} energy increases from 42 to 80 MeV. Assuming that the contributions from the higher spin states are small at 42 MeV, the fractional contribution to the total peak at 478 keV from the $6^{+}\rightarrow 4^{+}$ and $4^{+\prime}\rightarrow 4^{+}$ transitions may be deduced from the fractional change with O^{16} energy in the $(2^{+\prime}\rightarrow 2^{+})/(2^{+\prime}\rightarrow 0^{+})$ ratio. The errors inherent in this procedure, of course, are large.

3. Os^{190} *Nucleus*

As was the case for the two lighter isotopes discussed in the preceding sections, the first three excited states in the ground-state band, as well as two and possibly three members of the γ band of Os^{190} were excited in this measurement.

Previous Coulomb excitation studies have obtained $B(E2)$ values for the transition $2^{+}\rightarrow 0^{+}$ [32,33,25]; these have been confirmed by lifetime measurements.[35] In addition, the $2^{+\prime}$ and 4^{+} levels have been studied with Coulomb excitation.[25,32] A particular problem which occurs for this nucleus and adds to the difficulties of obtaining accurate determinations of $B(E2)$ values for the 4^{+} and $2^{+\prime}$ states is the near degeneracy of the $2^{+\prime}\rightarrow 2^{+}$ and $4^{+}\rightarrow 2^{+}$ transitions which cannot be resolved with a NaI(Tl) detector. These two transitions combine to form a composite peak near 365 keV in the NaI(Tl) γ-ray spectra.

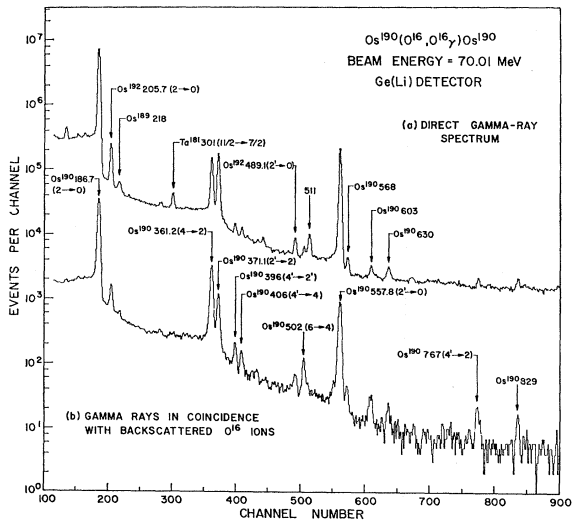

FIG. 7. γ-ray spectra obtained with a 22-cm² Ge(Li) detector following Coulomb excitation of 95.46% enriched Os^{190} with 70.01-MeV O^{16} ions: (a) direct singles spectrum; (b) spectrum taken in coincidence with backscattered O^{16} ions. The energy of the γ rays is given in keV. The spin change associated with each γ-ray transition is indicated in the figure. Some of the prominent transitions not originating from Coulomb excitation of Os^{190} have been identified in the figure.

Examples of NaI(Tl) spectra are presented in Fig. 6 where this feature is evident. The accompanying Fig. 7 shows data taken with a Ge(Li) detector which resolves this difficulty. To determine the excitation probabilities for the 4^{+} and $2^{+\prime}$ states at bombarding energies other than 70.01 MeV where no γ-particle coincidence data were taken with the Ge(Li) detector, the Ge(Li) data are used to obtain the branching ratio for the $2^{+\prime}$ state which decays via a 557.8-keV γ ray to the ground state and via a 371.1-keV γ ray to the 2^{+} state. The same ratio must also apply in the NaI(Tl) spectra and, coupled with the measured intensity of the 557.1 keV γ radiation, permits determination of the contribution to the 361.2–371.1 keV peak from the $2^{+\prime}\rightarrow 2^{+}$ deexcitations. The remainder of the peak in the NaI(Tl) spectra reflects the depopulation of the 4^{+} state. As in all the NaI(Tl) spectra obtained in this investigation, there are corrections to be made to all the intense peaks reflecting transitions from higher excited states which are unresolved with NaI(Tl). However, except for the highest bombarding energies used, these corrections are small, and in those cases where they are important, the Ge(Li) data may be used to good advantage.

Three deexcitations of the $4^{+\prime}$ state are observed: $4^{+\prime}\rightarrow 2^{+\prime}$, $4^{+\prime}\rightarrow 4^{+}$, and $4^{+\prime}\rightarrow 2^{+}$, identified by their close correspondence in energy with previously established transitions in Os^{190} and by initial and final spin determination from angular distribution studies of the γ rays in γ-particle coincidence measurements. The 767-keV $(4^{+\prime}\rightarrow 2^{+})$ transition is also discernible in the Na(Tl) data, and provides a crude measurement of the excitation probability for the $4^{+\prime}$ state as a function of the bombarding energy. The branching ratio for the decay of this state agrees fairly well with the data from other available studies involving radioactive decay. However, there remains an uncertainty in assigning the strength for the $4^{+\prime}\rightarrow 4^{+}$ transition because of a possible contribution from a $\sim$406-keV γ ray whose origin may be a state at 1161 keV which has previously been described[15,17,19] as a $K=I=4^{+}$ two-phonon γ vibration. An accompanying branch from the 1161-keV state decay is a 604-keV[4] transition which may be associated with a γ ray of that energy seen in the γ-particle Ge(Li) spectrum shown. However, no definite assignments can be made from these data for the 604-keV γ ray, so that the branching ratios for the $4^{+\prime}$ state as presented here are calculated by assigning the total strength of the 407-keV γ ray to the $4^{+\prime}\rightarrow 4^{+}$ transition.

The 502-keV γ ray seen in the Ge(Li) γ-particle spectrum has been identified with the $6^{+}\rightarrow 4^{+}$ transition. The γ-γ coincidence data establish that it is in coincidence with the deexcitations from the 4^{+} and 2^{+} states.

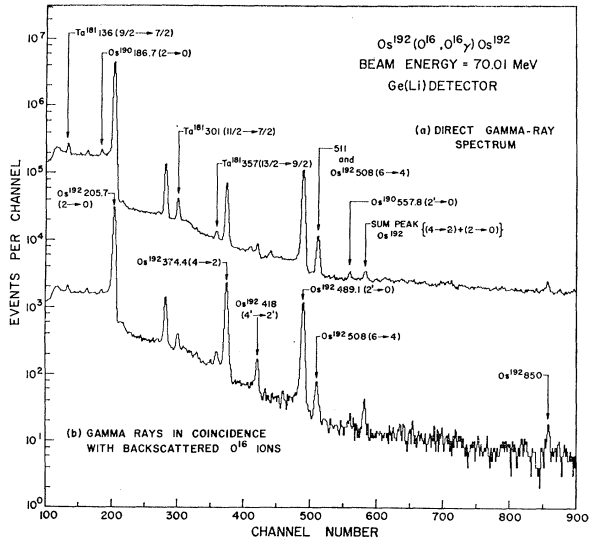

FIG. 8. γ-ray spectra obtained with a 22-cm^2 Ge(Li) detector following Coulomb excitation of 95.46% enriched Os^{192} with 70.01-MeV O^{16} ions: (a) direct singles spectrum; (b) spectrum taken in coincidence with backscattered O^{16} ions. The energy of the γ rays is given in keV. The spin change associated with each γ-ray transition is indicated in the figure. Some of the prominent transitions not originating from Coulomb excitation of Os^{192} have been identified in the figure.

The angular distribution of the γ ray in coincidence with backscattered ions verifies the spin sequence of the transition.

4. Os^{192} Nucleus

The dominant peaks in the Os^{192} spectra, examples of which are shown in Figs. 8 and 9, are at 205.7, 283.4, 374.4, and 489.1 keV. They correspond, respectively, to the $2^+\rightarrow 0$, $2^{+\prime}\rightarrow 2$, $4^+\rightarrow 2^+$, and $2^{+\prime}\rightarrow 0$ deexcitations. In addition to these levels, the only other state that has been previously identified in Os^{192} is the 3^+ state at 691 keV.

Aside from the weak sum peak at 580 keV, the other structure in the γ-particle data appears at 327, 418, 508 and 850 keV. Except for possibly the 850-keV peak whose origin is presently in question, it is evident from comparison of the γ-particle and singles Ge(Li) data that these peaks correspond to transitions which are enhanced, relative to a transition such as $2^+\rightarrow 0^+$, when the scattered coincident particles are selected in the backward direction. Such behavior normally implies that the state is being excited by multiple Coulomb excitation and most probably has a spin greater than 2^+ when the ground-state spin is 0^+. The sensitivity of the γ-γ coincidence data falls short of providing any information on these γ-rays because of the low yields and the poor resolution of the NaI(Tl) detectors. Studies of the angular distribution for γ rays in coincidence with backscattered particles are consistent, however, with assignments of $4^{+\prime}\rightarrow 4^+$, $4^{+\prime}\rightarrow 2^{+\prime}$, and $6^+\rightarrow 4^+$, respectively, for the 327-, 418-, and 508-keV γ rays. Associating the 6^+ state and the second 4^+ state with the third member of a ground-state band and the third member of a γ-vibrational band, respectively, is also consistent with the systematic evolution of the energy levels of the four Os nuclei. As will be discussed below, matrix elements for the above transitions if interpreted in this way, also show a systematic evolution with mass number. A disturbing feature, which may argue against the assignment of the $4^{+\prime}$ state to the γ-vibration band, is the absence of a detectable $4^{+\prime}\rightarrow 2^+$ transition at 701 keV; the corresponding transition was detected for the other three isotopes. The trend towards inhibition of crossover transitions as the properties of the four nuclei evolve from a rotational to a vibrational character, may, however, explain this discrepancy. The new 6^+ level would then occur at 1088 keV and the $4^{+\prime}$ level at 907 keV.

IV. REDUCED TRANSITION PROBABILITIES

For the reasons discussed in Sec. II, the reduced transition probabilities were obtained from the γ-backscattered-ion coincidence data. The procedure adopted for extracting $B(E2)$ values from these data was to compare measured and calculated Coulomb excitation probabilities for each level i, normalized to the Rutherford scattering yield. The transition matrix elements are adjustable parameters in the calculated probabilities, and are chosen to fit the experimentally determined probabilities. The obvious advantages of comparing experimental and calculated normalized excitation probabilities, instead of direct excitation yields, is evident in the reduced sensitivity of the excitation probability to uncertainties in some of the quantities that enter into the calculation of the expected Coulomb excitation yield. These include the beam

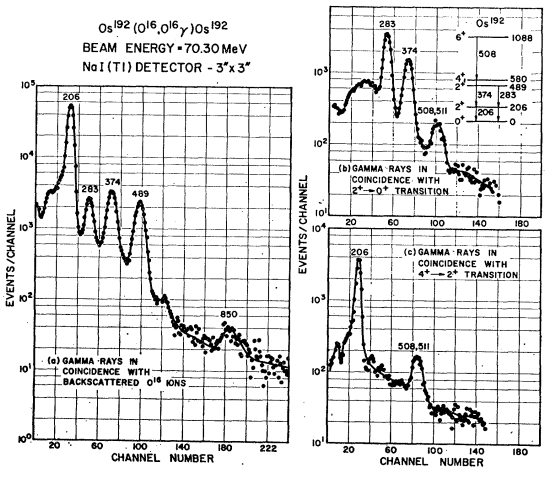

FIG. 9. NaI(Tl) γ-ray spectra following Coulomb excitation of 98.68% enriched Os^{192}: (a) spectrum taken in coincidence with backscattered O^{16} ions; (b) and (c) spectra taken in coincidence with the 206-keV ($2^+\rightarrow 0^+$) and 374-keV ($4^+\rightarrow 2^+$) transitions in the ground-state band.

energy, the angle and solid angle for the scattered particle, the specific ionization energy loss for the projectile, and the low-energy instrumental cutoff discussed in Sec. II A.

The average probability for exciting level i per ion scattered into the annular particle detector at an energy above the instrumentally determined cutoff energy E_c may be written

$$\bar{P}_i=\left(\int d\Omega\int_{E_c(\theta,i)}^{E_0}\frac{d\sigma_R}{d\Omega}(\theta,E)P_i(\theta,E)\frac{dE}{dE/ds}\right)$$

$$\times\left(\sum_i\int d\Omega\int_{E_c(\theta,i)}^{E_0}\frac{d\sigma_R}{d\Omega}(\theta,E)P_i(\theta,E)\frac{dE}{dE/ds}\right)^{-1},\quad(1)$$

where P_i is the excitation probability for the level i for a projectile of energy E_0 scattered through an angle θ, the quantity $d\sigma_R/d\Omega$ is the Rutherford scattering cross section, and dE/ds is the specific ionization-energy loss for the projectile obtained from interpolation in Z for the projectile obtained from interpolation in Z in the range-energy curves given by Northcliffe.[37] In the integral over the scattered-ion energy the low-energy cutoff $E_c(\theta,i)$, is the minimum energy an incident O^{16} projectile has to have just prior to excitation of level i in the target nucleus such that it can be scattered, at the most backward sensitive angle, into the particle detector with energy greater than E_m. The latter bias set by an electronic discriminator level serves to eliminate charged particles resulting from nuclear reactions rather than Coulomb excitation. It may be noted that E_c depends only slightly on the excitation energy of the state i, and that in the integration over the solid angle of the detector $d\Omega$, the use of a single mean scattering angle in lieu of an angular integration leads to possible errors of less than 1.5% in all cases treated here. The calculation of theoretical averaged excitation probabilities is in this way reduced to the evaluation of the excitation probability amplitudes. For sufficiently low incident energy, these may be obtained from first- and second-order perturbation theory. However, for higher bombarding energies, with the consequent strong excitation of many levels, all matrix elements connecting all levels involved in the excitation process must be known for an accurate evaluation of the excitation amplitudes. This can be accomplished either by resorting to model-dependent multiple Coulomb excitation theory[38,39] or by solving the full set of coupled Schrödinger equations for the excitation amplitudes. The former method relates the matrix elements through a specific model; both this and perturbation theory analysis have been applied to a preliminary version of these data[36] and $B(E2)$ values for the excitation of the low-lying states have been extracted.[40] In the latter procedure, when used in the most general way, the full set of matrix elements are considered as independent input parameters in the calculated probabilities and are varied to fit the measured $\bar{P}_i$. The virtues of the last approach are obvious; within the framework of the Coulomb excitation theory used it is exact, is model-independent, and in principle is capable of dealing with states of unspecified character. In practice, as the complexity of the energy-level system to be analyzed increases, the variety of experimental information required for a unique solution for the matrix elements becomes more demanding. In typical situations where a number of levels are involved, data with different projectile species and a variety of projectile energies are needed to permit a unique solution for the off-diagonal and diagonal matrix elements. By successively increasing the complexity of the system, as the projectile mass and energy are increased, unique solutions can be obtained for most of the matrix elements. In particular, in these investigations, it was found that the set of matrix elements required to fit the experimental results at a given incident energy was not unique, but that if data at several energies were available, a unique set could be obtained with the aid of some simplifying and plausible assumptions which are discussed below. Also discussed below are some of the uncertainties arising from lack of some experimental information.

In these analyses, we used the Winther and de Boer code,[41] which numerically solves the coupled Schrödinger equations representing the time-varying interaction between the projectile and nucleus in the semiclassical approximations. The input data consist of the bombarding conditions, energies and spins of all nuclear levels involved, and the full set of $E2$ matrix elements connecting all the levels considered in the calculation. For the thick-target integrations required in much of the analysis performed here, the code was modified to perform the required energy integrations and to allow immediate evaluation of the probabilities $\bar{P}_i$. Additional input data for this modified code consisted of the values for $E_c(\theta,i)$ and of coefficients arising in the empirically determined expression for dE/S.

For the matrix elements relevant to transitions among the ground and first few excited states (2^+, 4^+

[37] L. G. Northcliffe, Natl. Acad. Sci. Natl. Res. Council Publ. No. **1133**, 173 (1956).

[38] K. Alder and A. Winther, Kgl. Danske Videnskab Selskab, Mat.-Fys. Medd **32**, No. 8 (1960); K. Alder, in *Proceedings of the Third Conference on Reactions Between Complex Nuclei, Asilomar, 1963*, edited by A. Ghiorso, R. M. Diamond, and H. E. Conzett (University of California Press, Berkeley, Calif., 1963); I. Berson, Nucl. Phys. **67**, 296 (1965).

[39] R. Lutken and A. Winther, Kgl. Danske Videnskab Selskab, Mat.-Fys. Medd **2**, No. 6 (1964).

[40] Differences between the $B(E2)$ values quoted in Ref. 36 and the $B(E2)$ values listed in Table I derive, in part, from the different analysis procedures used in the two cases, as discussed in the text. In addition, the new and more comprehensive measurements, performed under conditions of improved resolution, reveal a number of previously undetected weak transitions which, if taken in account, modify some $B(E2)$ values and branching ratios given in Ref. 36.

[41] A. Winther and J. de Boer, in *Coulomb Excitation*, edited by K. Alder and A. Winther (Academic Press Inc., New York, 1966), p. 303.

and $2^{+\prime}$), the results from first- and second-order perturbation theory analysis of the data taken at the lowest bombarding energies were used as starting points in the computer search to fit the measured excitation probabilities; rotational-model matrix elements were chosen as first approximations in the search for matrix elements connecting the higher-lying states of the ground state and γ bands (6^+, 8^+, $4^{+\prime}$, and $6^{+\prime}$). The effect of high-lying unobserved states on the excitation probabilities of the observed states in each band was studied in the approximation that only the next highest unobserved members of each band (8^+ and $6^{+\prime}$) are considered to have a significant effect on the excitation probabilities of the observed states. Exploration with rotational-model values for the matrix elements connecting the observed states with the two unobserved states indicated that the effects are not large in the cases considered here and were effectively within the experimental uncertainties. Where these effects were necessarily taken into account, for consistency, use was made of the rotational-model matrix elements, modified by rotational-vibrational coupling as determined from data on branching ratios. Other transitions which were observed in this work but not definitely identified, or other states unobserved in this experiment but known to be present from reaction and decay scheme investigations, were not included in these analyses. It is expected that the omission of these states will not have a significant effect on the final matrix elements obtained.

There are two other important considerations in the analysis procedure which involve adoption of certain assumptions related to the quadrupole moments of the various states (diagonal matrix elements) and the signs of all the matrix elements, respectively.

Since only one projectile species was used in these experiments, no direct information is easily available from these measurements on the diagonal matrix elements, which in turn introduces uncertainties in the evaluation of the $B(E2)$ values. An analysis of the data using the computer code indicates that varying the values of the quadrupole moments in the analysis between zero and the Kumar and Baranger predictions changes the $B(E2)$ values extracted from the measured excitation probabilities by a few percent for the lowest-lying states such as the $2^{+\prime}$ state in the γ band. We note also that the Kumar and Baranger calculations predict values for the quadrupole moments which vary from 0.9 to about 0.25 times the rotational-model values as one proceeds from Os^{186} to Os^{192}; this fraction is almost constant for all the levels being considered of a given nucleus. Therefore, if the actual quadrupole moments are as large as the rotational-model values, then the contribution to the excitation of a given level, by virtue of its finite quadrupole moment, is even larger than cited above.

In the light of the comparisons to be made below, it is very likely that the quadrupole moments will be within the range determined by the rotational model values and the values calculated by Kumar and Baranger. Partial corroboration of this conclusion is provided by the results obtained in recent measurements by Saladin and co-workers[42] of the reorientation effect in the Coulomb excitation of the 2^+ state in Os^{190} and Os^{192}. The values calculated by Kumar and Baranger agree with the values for the quadrupole moments that have been extracted from these data. With the absence, for the present, of any further experimental information on the quadrupole moments for the other states of interest, we have adopted the point of view that the actual values for the quadrupole moments lie between the two model predictions that are being discussed. In particular, for consistency we have used the values calculated by Kumar and Baranger in our analysis, since those values seem to agree with existing data on quadrupole moments, and since, as is discussed below, the results of calculations using this model most comprehensively reproduce a large body of experimental data. The error that may be introduced into the evaluation of the $B(E2)$ values from the data due to uncertainties in the quadrupole moments may be estimated by considering that a 30% uncertainty in the quadrupole moment chosen translates typically into possible errors from this source in the $B(E2)$ values of approximately 1–6%, depending on the particular state involved. In Os^{186} and Os^{188}, the quadrupole moments predicted by the two models differ by less than 3%. In Os^{190} and Os^{192} the differences in model predictions for the quadrupole moments are larger; however, as discussed above, some measurements are available for these nuclei which lends evidence to the values used in the analysis. (It should be noted that the quadrupole moment values for the first 2^+ states in the neighboring even isotopes of Pt predicted by Kumar and Baranger agree with the measured values,[42] and that their calculation successfully predicts the change in the quadrupole moment sign found in Os^{192} and Pt^{194}.) It is difficult to assign the error contributed to the $B(E2)$ values that derive from uncertainties in the quadrupole moments chosen. On $Os^{186,188,190}$ an error corresponding to a $\pm 30\%$ uncertainty on the moments chosen appears liberal, while in Os^{192} a similar uncertainty may still be appropriate but more arbitrary. We have included errors arising from a $\pm 30\%$ uncertainty in the quadrupole moments in Table I.

In the question of the signs of the matrix elements, the choice of sign for most of the matrix elements has no effect on the excitation probabilities. Only in those cases in which a state may be excited by more than one common route, and in which interference terms may thus arise, containing combinations of products of matrix elements, do the choices of relative sign of matrix elements have significant effects on the excitation

[42] R. J. Pryor, J. X. Saladin, J. R. Kerns, and S. Lane, Bull. Am. Phys. Soc. **14**, 123 (1969); R. J. Pryor (private communication).

TABLE I. Summary of the best-fit $B(E2)$ values obtained by fitting both the thin- and thick-target measured excitation probabilities as a function of O^{16} ion energy. The Winther–de Boer code (Ref. 43) was used to calculate the theoretical $\bar{P}_i$ values of Eq. (1). Internal conversion coefficients were taken from calculations by Sliv and Band (Ref. 43). Assumptions adopted on the diagonal matrix elements and relative signs of matrix elements are discussed in the text.

		$B(E2; i\to f)$ (10^{-48} e^2 cm^4)											
		Os^{186}			Os^{188}			Os^{190}			Os^{192}		
i	f	Expt	KB[a]	Rot model	Expt	KB[a]	Rot model	Expt	KB[a]	Rot model	Expt	KB[a]	Rot model
0^+	2^+	3.11±0.11[b]	2.950		2.75±0.15[b]	2.731		2.55±0.25[a]	2.595		2.21±0.22	2.576	
2^+	4^+	1.69±0.12	1.632	1.60	1.41±0.11	1.509	1.41	1.07±0.10	1.429	1.34	0.98±0.09	1.405	1.14
4^+	6^+	1.64±0.25		1.41	1.68±0.26		1.25	1.50±0.23		1.16	1.26±0.25		1.01
0^+	$2^{+\prime}$	0.244±0.024	0.190		0.250±0.022	0.184		0.220±0.020	0.143		0.215±0.019	0.035	
2^+	$2^{+\prime}$	0.107±0.011	0.256	0.0700	0.146±0.013	0.403	0.0715	0.245±0.022	0.539	0.0629	0.361±0.032	0.743	0.0615
2^+	$4^{+\prime}$	0.0255±0.0063		0.0525	0.020±0.004		0.0535	0.0187±0.0037		0.0472			0.0461
4^+	$4^{+\prime}$	0.176±0.053		0.0858	0.159±0.032		0.0875	0.362[d]±0.072		0.0772	0.367±0.184		0.0755
$2^{+\prime}$	$4^{+\prime}$	0.99±0.35[c]		0.666	1.05±0.35		0.589	0.878±0.180		0.546	0.312±0.062		0.474
2^+	$0^{+\prime}$				0.00612[e]±0.0015	0.022							

[a] KB indicates calculated values by Kumar and Baranger (Ref. 3).
[b] From Ref. 45.
[c] The transition $4^{+\prime}\to 2^{+\prime}$ was not observed in this experiment. The $B(E2; 2^{+\prime}\to 4^{+\prime})$ value was obtained by using the ratio $B(E2; 4^{+\prime}\to 2^{+\prime})/B(E2; 4^{+\prime}\to 2^+)=33.5\pm 8.4$ from Ref. 2.
[d] The possible contribution from the decay of the 4^+(1161 keV) state has not been deleted. See text, Sec. III 3.
[e] See discussion of this value in the text.

probability. For the $2^{+\prime}$ states, the interference term ranges from approximately 25% of the excitation probability in Os^{186} to about 7% in Os^{192}. A measurement of the beam-energy dependence of the excitation probability can, in principle, determine the sign of the interference term. The effects sought in typical cases are, however, small, so that only very precise measurements can be definitive. The precision achieved in our measurements does not conclusively determine the sign of the interference terms. However, the data provide some experimental confirmation for the choice of signs adopted below, insofar as the analysis shows that this choice leads to a set of $B(E2; 0^+\to 2^{+\prime})$ values that are more constant with a variation of O^{16} energy than does the other choice of sign for the interference term.

In all cases, the relative and absolute signs have been chosen in accord with the dictates of the rotational model for a nucleus with a prolate shape both in its ground and excited states. This assumption determines all the signs of the matrix elements except for the relative sign between transitions within a band and transitions between the γ and ground-state bands. This exception however is trivial, since the choice of the relative sign produces no effect on the excitation probabilities. The choice of a prolate shape is consistent with what is known for the Os nuclei,[42] and the general systematics of this region. It may be noted that, although the absolute magnitudes of the matrix elements may deviate from those of the rotational model, it probably remains a very good assumption that the signs may be correctly given by this model, as is evidenced by the strong rotational structure pattern in the energy level spectra of $Os^{186,188,190}$. In these nuclei, the ground-state rotational band structure persists at least through the 8^+ level and, in the γ band, states past the $4^{+\prime}$ level have also been observed. The argument may be less convincing for Os^{192}; however, even in this case the observation in this experiment of the 6^+ level in the ground-state band and of a $4^{+\prime}$ level, which is probably associated with the γ band, again strengthens the choice of matrix element signs. Finally it is noted that the Kumar and Baranger calculations predict the sign of the interference term in the excitation probability which we have on the above considerations.

In employing the Winther–de Boer code, most of the calculations were performed at a single mean particle scattering angle, and with inclusion of the $M=0$ magnetic substates only. These approximations resulted in uncertainties in the calculated excitation probabilities that are well below 1.5% in all cases except for the excitation of 6^+ and $4^{+\prime}$ states for which they are less than 3%. In the final fits leading to the entries in Table I, all required magnetic substates were included, and an integration was performed over the solid angle of the particle detector. As noted above, the question of uniqueness of the fit was largely eliminated by the availability of data over a broad range of projectile energies and the stipulation that a simultaneous fit be

made to all the data. In addition, the rapidly decreasing excitation probability as the energy-level excitation energy increases enables the analysis to proceed progressively from the lower to the higher levels with fairly small corrective feedback to the lower states from the inclusion of higher states. The limited coupling between states, when analyzed in this order, lends evidence to the uniqueness of the very large set of matrix elements generated.

The experimental excitation probabilities were obtained in a generally standard manner, from the spectra already described, by integrating the γ-ray yields under the photopeaks and applying correction factors related to detector efficiency, detector solid angle, analyzer dead time, backgrounds, absorber effects, cascading decays, internal conversion coefficients, isotopic target enrichments, and anisotropies in γ-ray angular distributions which are discussed in detail in Sec. V. In the γ-particle coincidence experiments, the effective particle-detector solid angle was calculated and corrected for center-of-mass motion; the energy cutoff for thick-target integrations was determined from a subsidiary calibration of the multichannel analyzer and calculated in a manner already described. Internal conversion coefficients were taken from the calculated tabulations of Sliv and Band[43] according to the usual relation

$$\alpha=\alpha_K+1.33\sum_{i=1}^{3}\alpha_{Li}.$$

In the case of the $2^+\rightarrow 0^+$ deexcitations of the first excited states in $Os^{186,188}$, a discrepancy exists between such theoretical coefficients and those observed.[44] The theoretical results have been used here; this constitutes a possible unavoidable additional source of error in the $B(E2; 0^+\rightarrow 2^+)$ values determined for these two nuclei.

$B(E2)$ values determined for each isotope from that set of matrix elements that results in the best fit to the experimental excitation probabilities at all measured projectile energies are presented in Table I, together with the results of the calculations by Kumar and Baranger[3] and the rotational-model predictions where applicable. Data obtained with the Ge(Li) detector were weighted most heavily in the analysis because of the detail available, particularly for the weak γ-ray transitions. In the final fits for $Os^{186,188,190}$, the $B(E2; 0^+\rightarrow 2^+)$ values were taken from the more precise measurements elsewhere carried out with α particles and protons[45]; this greater precision reflects the uncertainties introduced, in this experiment, by the large absorber corrections for finite target thickness that were necessary for γ rays below 200 keV in energy. The present measurements of $B(E2; 0^+\rightarrow 2^+)$, however, agree with the values quoted in Table I, although their probable errors are larger.

The $4^{+\prime}\rightarrow 2^{+\prime}$ transition in Os^{186} was not observed in these measurements. The entry in Table I is obtained from the measured branching ratio $(4^{+\prime}\rightarrow 2^{+\prime})/(4^{+\prime}\rightarrow 2^+)$ from Emery *et al.*[2] together with the intensity of the $4^{+\prime}\rightarrow 2^+$ transition measured in this experiment. Similarly, the $4^{+\prime}\rightarrow 2^+$ transition from the $4^{+\prime}$ state in Os^{192} was not detected. Since the decay of the $4^{+\prime}$ state has been observed for the first time in this work, this contribution to the $4^{+\prime}$ deexcitation was necessarily estimated from a model calculation. Use was made of the rotational model modified by rotational-vibration coupling as determined from the data on the branching ratios from the $2^{+\prime}$ state. As observed in the following discussion, for Os^{192} this procedure is probably a poor approximation, but it has only a small effect on the $B(E2)$ values deduced for the other transitions.

The $B(E2; 2^+\rightarrow 0^{+\prime})$ in Os^{188} listed in Table I was obtained by assuming that the population of the $0^{+\prime}$ state proceeds via the $0^+\rightarrow 2^+\rightarrow 0^{+\prime}$ excitation route only. Consideration of the additional excitation route $0^+\rightarrow 2^{+\prime}\rightarrow 0^{+\prime}$ introduces an interference term between the two routes which can considerably alter the $B(E2; 2^+\rightarrow 0^{+\prime})$ value from the one listed in Table I, although the direct excitation of the $0^{+\prime}$ state via the second route is itself weak. The sign of the interference term is unknown, so that the value listed for $B(E2; 2^+\rightarrow 0^{+\prime})$ must presently be considered only a qualitative estimate. It may be noted that choosing the sign for the interference term given by the Kumar and Baranger wave functions, yields a value for $B(E2; 2^+\rightarrow 0^{+\prime})$ in good agreement with their predicted value of 0.022.

An assessment of the accuracy with which the reduced transition probabilities deduced from the $B(E2)$ values listed in Table I can reproduce the experimental measurements over a wide range of projectile energies may be made from Fig. 10. Here the averaged excitation probability $\bar{P}_i$, defined in Sec. IV, is plotted for the levels 2^+, 4^+, and $2^{+\prime}$. The data points shown were obtained with a NaI detector. The solid lines are the calculated excitation probabilities using reduced transition probabilities from Table I. For the measurements on thick targets, the O^{16} energies plotted are not the bombarding energies but rather weighted mean energies, determined separately for each state. The calculated and experimental probabilities begin to deviate at the highest bombarding energies used, presumably reflecting the onset of nuclear reactions. These data points were omitted in the fitting procedures for the reduced transition probabilities. It is apparent that for the remaining data, the mean reduced transition probabilities produce very good fits although the corresponding probabilities sometimes vary over some 2 orders of magnitude.

V. ANGULAR DISTRIBUTIONS

For detection geometries used in this experiment where the scattered particles are detected in an annular counter symmetrically located about the beam direc-

[43] L. A. Sliv and I. M. Band, Report No. 57 ICC, Physics Department, University of Illinois (unpublished).
[44] S. C. Pancholi, Nucl. Phys. **67**, 203 (1965).
[45] P. H. Stelson and L. Grodzins, Nucl. Data **1**, 1 (1965).

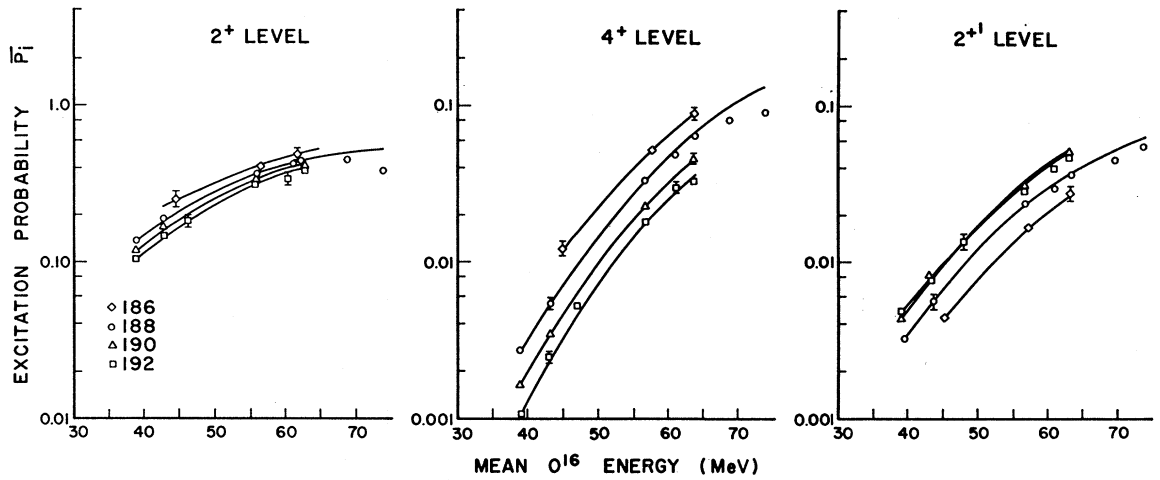

FIG. 10. Experimental excitation probabilities for the 2^+, 4^+ and 2^+ states versus O^{16} ion energy for thin and thick targets of $Os^{186,188,190,192}$. For the measurements on thick targets, the O^{16} ion energies plotted are not the bombarding energies but rather weighted mean energies, determined separately for each state, that would yield an excitation probability for a thin target equal to the measured value. The solid lines represent calculated excitation probabilities using the best fit $B(E2)$ values listed in Table I.

tion, it is well known that the angular distibution for the deexcitation γ rays, with multipolarities not greater than two, can be written as

$$W(\theta)=A_0+Q_2A_2P_2(\cos\theta)+Q_4A_4P_4(\cos\theta), \quad (2)$$

where Q_2 and Q_4 are attenuation coefficients reflecting the finite angular apertures of the γ detectors. For the NaI(Tl) detectors, they were obtained by interpolation from a tabulation by Yates,[46] while for the Ge(Li) counter, a computer calculation similar to Yates's was performed. The parameters A_2 and A_4 are, in general, functions of the Coulomb excitation parameter ξ, and therefore functions of the bombarding energy.

In a thick-target singles experiment, all the magnetic substates must be included in calculating A_2 and A_4, and integrations must be performed over the O^{16} ion scattering angle as well as over the thick-target energy interval specified by the projectile energy and the cutoff energy E_c. To avoid the long calculations which would have had to have been performed for an energy-level system with the complexity encountered in these experiments, all angular distribution corrections for the singles data were made empirically by performing detailed measurements at angular intervals of approximately 10° and subsequently summing data over all angles. The singles measurements were used principally for the extraction of branching ratios, and these measurements represent our most accurate determinations of these ratios.

In experiments in which the angular correlation of γ rays is measured in coincidence with the inelastically backscattered particles near 180°, the computational task decreases very significantly.[47] As previously mentioned in Sec. II, under these conditions, for a zero ground-state spin and a projectile with spin zero, the major contribution to the excitation probability derives from the $M=0$ magnetic substates; the integration of the scattered ion direction may be replaced by a scattering at the mean angle, and the angular distribution is largely independent of the value of the Coulomb excitation parameter ξ, eliminating the integration along the particle's path in the thick target. The dominance of the $M=0$ magnetic substates renders the angular distribution independent of the excitation mechanism. Added virtues for multipole determinations are the resulting large anisotropies, and large A_4 coefficients which frequently resolve the ambiguity in the choice between two values of the $E2/M1$ mixing ratio δ which characteristically arises in singles measurements where A_4 is small. Tests of the independence of $W(\theta)$ on incident energy and on excitation mechanism were made using the Winther–de Boer code with all five magnetic substates through $|M|=2$ considered. The independence was verified to within 1% for most of the states of interest in this experiment. Angular distribution measurements were performed in the 180° coincidence configuration for the more prominent $2^+\rightarrow 0^+$, $4^+\rightarrow 2^+$, $2^{+\prime}\rightarrow 0^+$ and $2^{+\prime}\rightarrow 0^+$ transitions using the NaI(Tl) detector at two bombarding energies, 48.26 and 70.30 MeV, and at three γ-detector angles, 0°, 45°, and 90° to the incident beam direction. More elaborate measurements were carried out at 70.01 MeV with the Ge(Li) detector, the results of which are shown in Fig. 11. All the data points have been corrected for

[46] M. J. Yates, Nucl. Instr. Methods **23**, 152 (1963).

[47] A. E. Litherland and A. J. Ferguson, Can. J. Phys. **39**, 788 (1961).

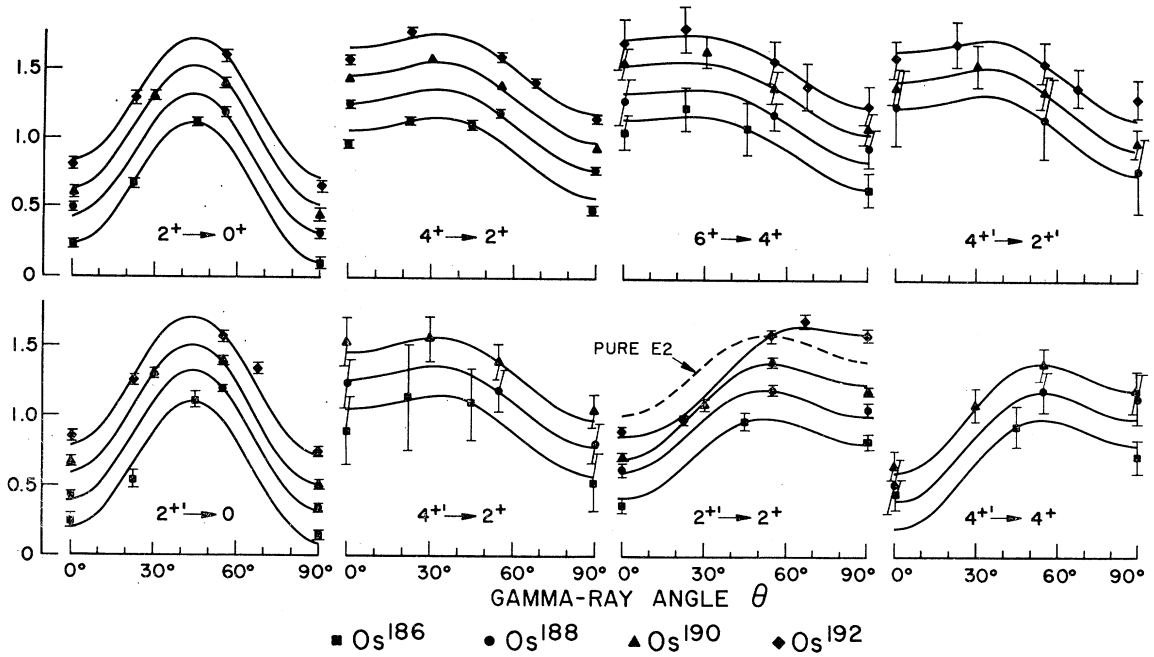

FIG. 11. Measured angular distributions of γ rays detected in coincidence with backscattered O^{16} ions. The angle θ is measured with respect to the direction of the incident O^{16} beam. The zero for the ordinate has been displaced by an arbitrary amount to separate the results for the four Os isotopes for clarity of presentation. The solid lines represent the best fits to the data. The coefficients A_2 and A_4 were deduced from these best fits.

cascading γ rays; thus, the angular distributions shown are for the circumstance in which the initial state involved in the deexcitation γ radiation is populated directly by Coulomb excitation. A sequential cascade subtraction procedure was followed by proceeding stepwise from the highest to the lowest transition in the cascade and making the appropriate corrections for the intensity and angular distributions for the cascading γ rays as determined by the Winther–de Boer computer program.

The solid lines in Fig. 11 for the $I \rightarrow I \pm 2$ transitions represent calculated angular distributions, suitably normalized, assuming the spin sequence shown and geometry attenuation factors calculated for the detector system used. (The zero has been sequentially displaced for each curve in a group for clarity of presentation.) The angular distribution patterns are very distinctive, so that the choice of spin sequence is generally unambiguous where coupled with other available information. The assignment of spins of 6 and 4 for the 1086- and 907-keV levels in Os^{192} are based partially on such measurements.

An analysis of the angular distribution for the $2^{+\prime} \rightarrow 2^+$ transitions established the magnitude and sign of δ for these transitions. The mixing ratio δ is defined here in the following way:

$$\delta = 0.835 E_\gamma \text{ (in MeV)} \times \frac{\langle 2 \,||\, M(E2) \,||\, 2' \rangle \text{ (in electron barns)}}{\langle 2 \,||\, M(M1) \,||\, 2' \rangle \text{ (in nuclear magnetons)}} \quad (3)$$

for the $2^{+\prime} \rightarrow 2^+$ transitions. The mixing ratio was deduced from the data on angular distributions by comparing the measured A_2 and A_4 coefficients with those calculated using the Winther–de Boer program allowing a finite δ. The results are given in Fig. 12 with the measured values for A_2 and A_4 indicated on the

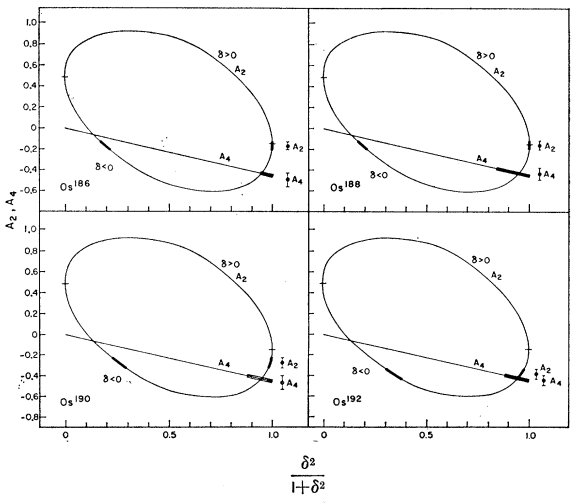

FIG. 12. Angular correlation coefficients A_2 and A_4 as a function of the $E2/M1$ mixing parameter δ, calculated for the $(2^{+\prime} \rightarrow 2^+)$ transitions in $OS^{186,188,190,192}$ following Coulomb excitation by backscattered O^{16} ions. The Winther–de Boer computer code was used to calculate the solid curves with $B(E2)$ values listed in Table I. The thick lines indicate the limits imposed on $\delta^2/(1+\delta^2)$ by the measured values for A_2 and A_4 shown in the figure.

TABLE II. Angular correlation coefficients A_2 and A_4 and $E2/M1$ mixing ratios, for the $(2^{+\prime}\rightarrow 2^+)$ transitions in $Os^{186,188,190,192}$. The experimental $B(M1)$ values were deduced from the measured mixing ratios and the measured $B(E2; 2^{+\prime}\rightarrow 2^+)$. The $B(M1)$ values listed under Kumar and Baranger were obtained using their mixing ratios and their predicted values for the $B(E2; 2^{+\prime}\rightarrow 2^+)$.

Nucleus	A_2	A_4	$(\delta)_{\text{expt}}$	$\frac{\langle 2\|\|M(E2)\|\|2'\rangle}{\langle 2\|\|M(M1)\|\|2'\rangle}$ (eb/μ_N) Expt	KB[a]	$B(E2; 2'\rightarrow 2)$ $(eb)^2$ Expt	KB[a]	$B(M1; 2'\rightarrow 2)$ $(10^{-4}\mu_N{}^2)$ Expt	KB[a]
Os^{192}	-0.390 ± 0.050	-0.451 ± 0.050	$-5.2(+1.6, -1.1)$	$-22.0(+6.8, -4.7)$	-22.0	0.361 ± 0.032	0.743	$7.45(+4.6, -3.1)$	15.4
Os^{190}	-0.275 ± 0.050	-0.469 ± 0.070	$-11(+6, -4)$	$-35.6(+19.4, -12.9)$	-24.5	0.245 ± 0.022	0.539	$1.94(+2.12, -1.40)$	8.99
Os^{188}	-0.157 ± 0.040	-0.437 ± 0.060	$\lvert\delta\rvert>30$	>75	-23.9	0.146 ± 0.013	0.403	<0.26	7.05
Os^{186}	-0.165 ± 0.040	-0.492 ± 0.070	$\lvert\delta\rvert>25$	>47	-27.9	0.107 ± 0.011	0.256	<0.49	3.28

$$\delta = 0.835\times(E_\gamma \text{ in MeV})\frac{\langle 2\|\|M(E2)\|\|2'\rangle \text{ (in } eb)}{\langle 2\|\|M(M1)\|\|2'\rangle \text{ (in } \mu_N)}$$

[a] KB indicates calculated values by Kumar and Baranger (Ref. 3).

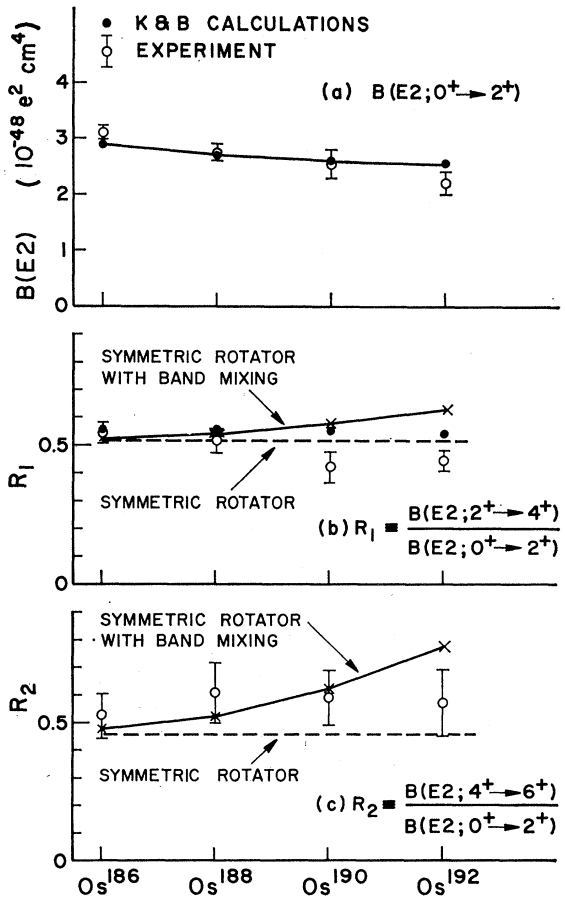

FIG. 13. $B(E2)$ values for transitions between members of the ground-state bands in $Os^{186,188,190,192}$. (a) Comparisons of the results of the Kumar and Baranger calculations with the measured $B(E2; 0^+\rightarrow 2^+)$ values. (b) Comparison of values for the ratios $B(E2; 2^+\rightarrow 4^+)/B(E2; 0^+\rightarrow 2^+)$ and $B(E2; 4^+\rightarrow 6^+)/B(E2; 0^+\rightarrow 2^+)$ predicted by the Kumar and Baranger calculations and the rotational model with band mixing with experimental ratios. The band mixing parameters used for the calculated values are taken from Table III.

figure. Because the magnetic substate population is dominated by $M=0$ in all the calculations, and the angular distributions are, therefore, to a very good approximation independent of the details of the excitation, one common set of coefficients A_2 and A_4 can be written numerically as functions of δ which are good approximations for all four isotopes of osmium:

$$A_2=(0.486+1.423\delta-0.149\delta^2)/(1+\delta^2), \quad (4)$$

$$A_4=0.490\delta^2/(1+\delta^2). \quad (5)$$

Table II summarizes the results for the four osmium isotopes, and compares δ and the $B(M1)$ values predicted by the Kumar and Baranger calculations with these measurements.[48]

[48] Measurements of δ for the $2^{+\prime}\rightarrow 2^+$ transition in $Os^{190,192}$ have recently been reported by Robinson *et al.*, Nucl. Phys. **123**, 193 (1969).

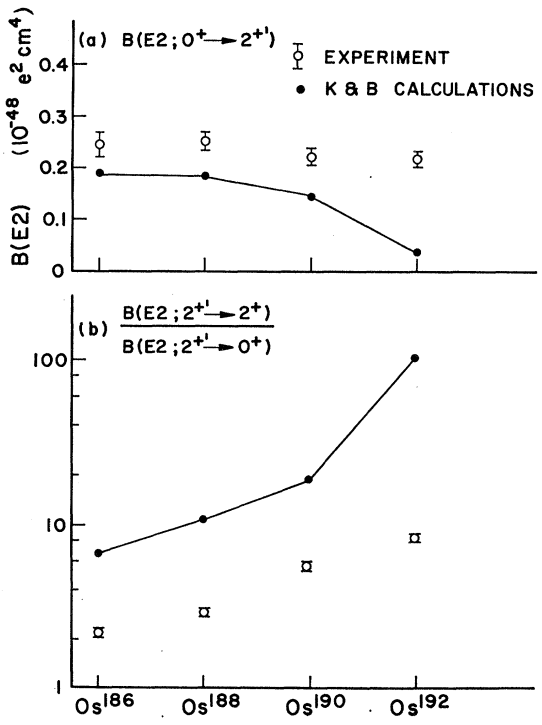

FIG. 14. Experimental and calculated values for (a) $B(E2; 0^+ \rightarrow 2^{+\prime})$ and (b) $B(E2; 2^{+\prime} \rightarrow 2^+)/B(E2; 2^{+\prime} \rightarrow 0^+)$ in $Os^{186,188,190,192}$ The solid lines join values predicted by the Kumar-Baranger calculations.

VI. DISCUSSION

One of the motivations for these measurements has been to provide the requisite experimental quantities for a detailed comparison with microscopic calculations in this region—in particular with those of Kumar and Baranger.[3] Such a comparison is presented in Tables I, II, and IV and Figs. 13 and 14. Calculated numerical results are only available for the 2^+, 4^+, $2^{+\prime}$, and $0^{+\prime}$ excited states so that our results for the 6^+ and $4^{+\prime}$ states cannot presently be compared with the microscopic calculations.

A physically revealing approach is to compare the results simultaneously with the predictions of the rotational model and the calculations of Kumar and Baranger. The predictions of the simple rotational model, with no rotation-vibration interaction, are included in Table I. The latter entries are obtained from the $B(E2; 0^+ \rightarrow 2^+)$ and $B(E2; 0^+ \rightarrow 2^{+\prime})$ values coupled with the assumption of equal intrinsic quadrupole moments for the ground- and γ-vibrational bands. Thus, two parameters are needed to specify the model's predictions for each nucleus. On the other hand, the Kumar and Baranger predictions require no special parameter fitting specific to each nucleus.

Refinements of the rotational model to include the rotation-vibration interaction are compared with experiment in Table III and in Fig. 13. Here at least one more parameter has to be introduced in a first-order band-mixing calculation to express the degree of mixing of the ground-state and γ-vibrational band wave functions. This first-order mixing results in a modification of the transition probabilities between states which follows a well-known angular momentum dependence.[49,50]

It should be mentioned that it is not clear that a band-mixing calculation is actually applicable in the osmium nuclei, since a first-order treatment may not be sufficient in view of the very large amount of mixing. Kumar and Baranger indeed find that the wave functions in $Os^{190,192}$ are actually smeared over large regions of the β-γ plane. As discussed below, even in $Os^{186,188}$, the preference for axial symmetry is not overwhelming in their model. We have included this discussion, however, with the viewpoint that it may stimulate some further insight.

We define the mixing parameter Z_2 here as follows[49]:

$$Z_2 = -(\sqrt{24})\epsilon_2 \, | \, Q_{00} \, | / | \, Q_{20} \, | . \qquad (6)$$

The reduced admixed amplitude ϵ_2 is obtained from the matrix element which mixes the γ-vibrational and ground-states bands. The quantities $| \, Q_{00} \, |$, $| \, Q_{20} \, |$, and $| \, Q_{22} \, |$ as well as the sign convention for Z_2 used in Table III are defined through the reduced transition probabilities $B(E2; 2^+ \rightarrow 0^+)$, $B(E2; 2^{+\prime} \rightarrow 0^+)$ and $B(E2; 4^{+\prime} \rightarrow 2^{+\prime})$:

$$B(E2; J_i, K_i \rightarrow J_f, K_f) = | \, Q_{K_i K_f} \, |^2 \langle J_i 2 K_i K \, | \, J_f K_f \rangle^2 \times f(\epsilon_2, \alpha_2, \alpha_2', J_i, J_f), \qquad (7)$$

where, $\alpha_2 = | \, Q_{00} \, | / | \, Q_{20} \, |$ and $\alpha_2' = | \, Q_{22} \, | / | \, Q_{20} \, |$. If in the correction term to the leading order matrix element it is assumed that $\alpha_2' = \alpha_2$, then the correction factors for the above transitions can be written as follows:

$$\begin{aligned} & f(Z_2, J_i, J_f) \\ & = (1 + Z_2/\alpha_2^2)^2 \quad \text{for} \quad K_i = K_f = 0, J_i = 2, J_f = 0 \\ & = (1 - Z_2)^2 \quad \text{for} \quad K_i = J_i = 2, J_f = K_f = 0 \\ & = (1 - 2Z_2/\alpha_2^2)^2 \quad \text{for} \quad K_i = 2, J_i = 4, K_f = J_f = 2. \end{aligned} \qquad (8)$$

The quantities $| \, Q_{K_i K_f} \, |$ are proportional to the intrinsic moments. Under the rotational-model assumptions, since it depends only on the internal state of the nucleus, $| \, Q_{20} \, |$ is constant for all transitions (J_i, $K = 2 - J_f$, $K = 0$), and the ratio $| \, Q_{22} \, | / | \, Q_{00} \, |$ yields directly the

[49] O. B. Nielsen, in *Proceedings of the Rutherford Jubilee Conference on Nuclear Physics*, edited by J. B. Birks (Heywood and Company, Ltd., London, 1962), p. 137.

[50] O. Nathan and S. G. Nilsson, in *Alpha- Beta- and Gamma-Ray Spectroscopy*, edited by Kai Siegbahn (North-Holland Publishing Co., Amsterdam, 1965).

TABLE III. Parameters deduced from the experimental data on branching ratios and absolute $B(E2)$ values both for the rotational model with rotational-vibrational coupling and the Davydov-Chaban model (Ref. 53). The three listings for the ratio $|Q_{22}|/|Q_{00}|$ refer to the three methods used to calculate this ratio, described in the text. The band-mixing parameters Z_2 and Z_2' were obtained from the branching ratios from the $2^+{}'$ and $4^+{}'$ states, respectively.

Nucleus	Intensity ratio $\frac{I(2'\to2)}{I(2'\to0)}$	$\frac{B(E2;2'\to2)}{B(E2;2'\to0)}$ Expt	KB[a]	Z_2[b]	Intensity ratio $\frac{I(4'\to4)}{I(4'\to2)}$	$\frac{B(E2;4'\to4)}{B(E2;4'\to2)}$ Expt	Z_2'[b]	$\lvert Q_{00}\rvert/\lvert Q_{20}\rvert$	c	$\lvert Q_{22}\rvert/\lvert Q_{00}\rvert$ d	e	μ[f]	γ[f]
Os^{186}	0.817±0.041	2.20±0.11	6.74	0.074±0.010	1.85±0.46	12.4±3.7	0.085±0.013 or 0.385±0.031	3.30±0.18	1.22±0.22	1.25±0.23	1.14±0.20	0.26	16°
Os^{188}	0.718±0.035	2.92±0.15	10.95	0.125±0.010	1.11±0.28	14.3±3.6	0.093±0.013 or 0.370±0.020	2.90±0.15	1.33±0.23	1.39±0.24	1.52±0.30	0.25	19°
Os^{190}	0.726±0.036	5.57±0.28	18.85	0.246±0.010	1.45±0.36	34.8±8.7	0.125±0.011 or 0.300±0.015	2.57±0.17	1.27±0.14	1.42±0.16	1.52±0.25	0.25	21°
Os^{192}	0.564±0.028	8.39±0.40	106.1	0.315±0.010				2.20±0.15	0.81±0.08	0.99±0.10	1.29±0.35	0.25	25.2°

[a] KB indicates calculated values by Kumar and Baranger (Ref. 3).
[b] Z_2 obtained from $B(E2;2'\to2)/B(E2;2'\to0)$; Z_2' obtained from $B(E2;4'\to4)/B(E2;4'\to2)$.
[c] Value obtained from $B(E2;2'\to4')/B(E2;0\to2)$ without band-mixing corrections.
[d] Value obtained from $B(E2;2'\to4')/B(E2;0\to2)$ with band-mixing corrections.
[e] Value obtained from double ratio Eq. (9).
[f] Davydov-Chaban model parameters obtained from the energy ratios E_4+/E_2+ and E_2+'/E_2+; Ref. 53.

TABLE IV. Comparison of ground-state-band-reduced-transition probabilities with the predictions of the rotational model and the Kumar-Baranger calculations. $R_1=B(E2;2^+\to4^+)/B(E2;0^+\to2^+)$; $R_2=B(E2;4^+\to6^+)/B(E2;0^+\to2^+)$.

Nucleus	$(R_1)_{expt}$	$(R_1)_{expt}$[a]$/(R_1)_{KB}$	$(R_1)_{expt}$[b]$/(R_1)_{rot}$	$(R_1)_{expt}$[c]$/(R_1)_{B.M.}$	$(R_2)_{expt}$	$(R_2)_{expt}$[d]$/(R_2)_{rot}$	$(R_2)_{expt}$[c]$/(R_2)_{B.M.}$
Os^{186}	0.545±0.043	0.99±0.08	1.06±0.08	1.04±0.08	0.527±0.082	1.16±0.18	1.09±0.18
Os^{188}	0.513±0.050	0.93±0.09	1.00±0.09	0.95±0.09	0.611±0.101	1.34±0.22	1.17±0.19
Os^{190}	0.420±0.059	0.76±0.11	0.82±0.12	0.73±0.10	0.588±0.108	1.29±0.24	0.94±0.18
Os^{192}	0.443±0.044	0.81±0.08	0.86±0.09	0.70±0.07	0.570±0.117	1.25±0.26	0.735±0.16

[a] $(R_1)_{KB}$ indicates calculated values by Kumar and Baranger (Ref. 3).
[b] $(R_1)_{rot}=0.514$.
[c] $(R_1)_{B.M.}$ and $(R_2)_{B.M.}$ indicate rotational model values corrected for band mixing.
[d] $(R_2)_{rot}=0.455$.

ratio of the intrinsic static quadrupole moments for the γ-vibrational and ground-state bands. In Table III, the ratio $|Q_{22}|/|Q_{00}|$ has been calculated using two methods. The first of these involves directly the measured reduced transition probabilities $B(E2; 2^{+\prime}\rightarrow 4^{+\prime})$ and $B(E2; 0^{+}\rightarrow 2^{+})$. The two entries in the table under this heading consist of the unmodified ratio $B(E2; 2^{+\prime}\rightarrow 4^{+\prime})/B(E2; 0^{+}\rightarrow 2^{+})$, and this ratio with correction terms for band mixing; the latter effects of band mixing, however, are small since they involve corrections of the order Z_2/α_2^2. This method is the more direct one with the minimum dependence on the model assumptions.

In the second method, $|Q_{22}|/|Q_{00}|$ is obtained from the following ratios of $B(E2)$ values, with the assumption stated above that transitions from the $4^{+\prime}$ and $2^{+\prime}$ states to the ground-state band are both determined by $|Q_{20}|$:

$$\left|\frac{Q_{22}}{Q_{00}}\right|^2 = 2.946\,\frac{B(E2; 4^{+\prime}\rightarrow 2^{+\prime})}{B(E2; 4^{+\prime}\rightarrow 4^{+})} \times \frac{B(E2; 2^{+\prime}\rightarrow 2^{+})}{B(E2; 2^{+}\rightarrow 0^{+})}\,\frac{(1+Z_2/\alpha_2^2)^2}{(1-2Z_2/\alpha_2^2)^2}. \quad (9)$$

This particular combination of $B(E2)$ values is chosen to reduce the influence of band mixing corrections which arise principally from the transitions between bands. In this expression the mixing corrections cancel to first order, therefore minimizing the influence of errors in Z_2. Since Eq. (9) involves only the branching ratio from the $4^{+\prime}$ state and the reasonably accurately measured $B(E2)$ to the $2^{+\prime}$ state instead of the more circuitally deduced $B(E2; 4^{+\prime}\rightarrow 2^{+\prime})$, the second method inherently can yield a more accurate determination of $|Q_{22}|/|Q_{00}|$ than can the first. However, it must be emphasized that in addition to the assumption of a constant $|Q_{20}|$ for a interband transitions, Eq. (9), which is based on the band-mixing model, tacitly assumes that the Z_2, as obtained from the branching ratio of the $2^{+\prime}$ states, is identical to the Z_2 obtained from the decay of the $4^{+\prime}$ states. This consistency is by no means clear for all the Os isotopes listed in Table III. The value for Z_2 used in all the calculations has been deduced from the ratio $B(E2; 2^{+\prime}\rightarrow 2^{+})/(B(E2; 2^{+\prime}\rightarrow 0^{+})$. Examination of the $|Q_{22}|/|Q_{00}|$ values listed in Table III indicates that, although the errors in the measurement are large, both methods yield values for this ratio which tend to be larger than unity.

A. Ground-State Band Transitions

Comparison of the models with the data for the ground-state band transitions are made in Table IV and are illustrated graphically in Fig. 13. The ratios R_1 and R_2 are defined as follows:

$$R_1 = B(E2; 2^{+}\rightarrow 4^{+})/B(E2; 0^{+}\rightarrow 2^{+}), \quad (10)$$

$$R_2 = B(E2; 4^{+}\rightarrow 6^{+})/B(E2; 0^{+}\rightarrow 2^{+}), \quad (11)$$

and $(R_{1,2})_{\rm rot}$ and $(R_{1,2})_{\rm B.M.}$ denote, respectively, the simple rotational-model predictions and the rotational model predictions modified by band mixing,

$$(R_1)_{\rm B.M.} = (R_1)_{\rm rot}[1+(5/3)Z_2/\alpha_2^2]^2 = 0.5143[1+(5/3)Z_2/\alpha_2^2]^2, \quad (12)$$

$$(R_2)_{\rm B.M.} = (R_2)_{\rm rot}[1+(14/3)Z_2/\alpha_2^2]^2 = 0.4545[1+(14/3)Z_2/\alpha_2^2]^2. \quad (13)$$

The Kumar and Baranger calculations reproduce the $0^{+}\rightarrow 2^{+}$ transition matrix elements both in absolute magnitude and their trend with neutron number. For the 4^{+} levels, these calculations are in satisfactory accord with experiment for $Os^{186,188}$, but differences begin to arise in $Os^{190,192}$, where the $B(E2)$ values predicted are larger than those measured. Generally, for the ground-state band, the fits are not noticeably better than those of the simple rotational model. Band mixing corrections to the rotational model only further increase the discrepancy between model and experiment. As mentioned earlier, numerical results for the Kumar and Baranger calculations are presently not available for the 6^{+} levels, so that the data on these levels cannot be compared with their model. A comparison with the simple rotational-model predictions shows that the model anticipates $B(E2; 6^{+}\rightarrow 4^{+})$ values that are too small. The addition of the first-order band-mixing correction to the model increases the model $B(E2; 6^{+}\rightarrow 4^{+})$ values above the experimental values for Os^{190} and Os^{192} in a manner which parallels the $B(E2; 4^{+}\rightarrow 2^{+})$ values for these two nuclei. The latter point is illustrated in Table IV. In general, as expected, the deviations from the model prediction increase as Os^{192} is approached. However, it is interesting to note that the rotational character of the low-lying energy-level spectrum is still quite pronounced even for Os^{192} as is evidenced by these comparisons.

Some insight into the structure of the ground-state bands is provided by consideration of the potential wells and wave functions calculated by Kumar and Baranger and displayed graphically in Ref. 3. In $Os^{186,188}$, the potential has a significant minimum (several hundred keV) for a prolate deformation and the ground-state wave function is strongly centered about this deformation. In $Os^{190,192}$, the potential minimum is much shallower ($\leq$150 keV), with zero-point motion being sufficient to smear out the wave functions. A moderately axially asymmetric equilibrium configuration is also favored. Progressing towards Os^{192}, the first 2^{+} states contain successively larger $K=2$ components in their wave functions. The differences in structure among the four isotopes, however, are not severe, and it is thus reasonable that a rotational picture only gradually loses merit as this transition region is traversed.

B. Interband Transitions

The significant differences between the Kumar and Baranger and the simple rotational-model predictions arise when their respective predictions for interband matrix elements are considered. The experimental branching ratios for the $2^{+\prime}$ state as well as the model predictions are listed in Table III. Figure 14 compares the measured $B(E2; 0^+\rightarrow 2^{+\prime})$ values and the ratio $B(E2; 2^{+\prime}\rightarrow 2^+)/B(E2; 2^{+\prime}\rightarrow 0^+)$ with the calculations. The simple rotational model is, of course, totally unable to account for the decrease in the $B(E2; 0^+\rightarrow 2^{+\prime})$ values relative to the $B(E2; 2^+\rightarrow 2^{+\prime})$ values as the vibrational limit is approached in Os^{192}. On the other hand, the Kumar-Baranger model successfully reproduces this general trend, and adequately accounts for some of the absolute $B(E2; 0^+\rightarrow 2^{+\prime})$ values. However, the model in its original form makes the transition from deformed to spherical shape more rapidly than appears to be the case experimentally; this results in calculated 2^+ states wave functions that have excessively large $K=2$ components in $Os^{190,192}$ and $B(E2; 0^+\rightarrow 2^{+\prime})$ values that are too small in these nuclei. In a phenomenological approach, one can consider modification of the potentials in Ref. 3 which would improve this situation. It is apparent that only a minor deepening of the prolate potential minima in $Os^{190,192}$ would slow the transition from deformed to spherical shape. The wave functions would not be nearly as smeared out in the β-γ plane, the first excited 2^+ state would contain less $K=2$ component, and in general, there would be less overlap of the calculated wave functions with those of the harmonic oscillator model. These changes would increase the $B(E2; 0^+\rightarrow 2^{+\prime})$ values in $Os^{190,192}$ and bring the $2^{+\prime}$ state branching ratios more into agreement with the experimental results. Such modifications can be effected by small variation in the relative strength of the pairing and quadrupole nucleon-nucleon residual forces assumed as input to the microscopic calculations.

Other microscopic calculations such as those of Bès[51] and Bès *et al.*[52] are also available for the osmium nuclei. These authors calculate $B(E2; 0^+\rightarrow 2^{+\prime})$ values. The latter nonadiabatic calculations by Bès *et al.* which include effects due to the Coriolis force, actually arrive at conditions of γ instability in $Os^{188,190,192}$, and consequently can only yield a $B(E2; 0^+\rightarrow 2^{+\prime})$ value for Os^{186}. The result obtained for this quantity is $0.51\times 10^{-48}e^2$ cm^4, about twice the experimental value. The former adiabatic calculations of Bès, however, finds large root-mean-square values of γ (but not γ instability) in $Os^{186,188,190}$, and hence can calculate $B(E2; 0^+\rightarrow 2^{+\prime})$ values for these three isotopes, obtaining 0.22, 0.23, and 0.37 ($\times 10^{-48}e^2$ cm^4), respectively. These numerical results are in better accord with our results than the latter, more general theory, but the trend is opposite to the experimental one.

We have also seen that the tendency towards an axially asymmetric structure for the calculated wave functions in $Os^{190,192}$ mentioned above finds support in the macroscopic model involving band mixing referred to earlier. In order to fit experimental branching ratios for the $2^{+\prime}$ and $4^{+\prime}$ states, the rotational model requires large mixing of $K=2$ components into the wave functions for the ground band member wave functions. It may also be noted that a comparison with the Davydov-Chaban model[53] likewise demonstrates that reproduction of experimental quantities, $B(E2)$ values, and energy levels in $Os^{186,188,190,192}$ requires large values of the softness parameter μ and generally increasing equilibrium axial asymmetry as measured by γ (see Table III).

C. *E2-M1* Admixtures

A further sensitive test of the Kumar-Baranger nuclear wave functions can be provided by the data on the $E2/M1$ mixing ratio in the $2^{+\prime}\rightarrow 2^+$ transitions.[54] In Table II, we see that while the agreement between the calculated and measured mixing ratios in Os^{190} and Os^{192} is reasonably good, the Kumar-Baranger calculations predict larger $M1$ admixtures in Os^{188} and Os^{186} than observed. The significance of these comparisons for the present, however, is questionable, since it has been pointed out by the author of the calculations that the numerical accuracy for nearly forbidden transition matrix elements is poor, and, the assumptions of the treatment may be particularly serious for $M1$ matrix elements.[54] A more meaningful comparison awaits a refinement in the calculations.

D. 0^+ States

A potentially major shortcoming of existing microscopic calculations is that they all indicate the existence of 0^+ excitations in all four Os nuclei in the region between 700 and 1500 keV. In particular, the Kumar-Baranger calculations predict these levels to exist near the lower end of this energy range. States with spin and parity 0^+ have been observed in Os^{188} at 1086 and 1765 keV,[6,13,14] and in Os^{190} at 912.4 keV.[55,56] Except for the 1086-keV 0^+ state in Os^{188}, such states have not been observed in this experiment with any certainty in the other three isotopes. This failure may only be apparent since the $B(E2)$ values for the excitation of these states is expected to be small and the states are difficult to

[51] D. Bès, Kgl. Danske Videnskab Selskab, Mat.-Fys. Medd **33**, No. 2 (1961); D. Bès, Nucl. Phys. **49**, 544 (1963).
[52] D. Bès, P. Federman, E. Maqueda, and A. Zuker, Nucl. Phys. **65**, 1 (1965).
[53] A. S. Davydov and A. A. Chaban, Nucl. Phys. **20**, 499 (1960).
[54] K. Kumar, Phys. Letters **29B**, 25 (1969).
[55] M. A. Mariscotti, W. R. Kane, and G. T. Emery, Bull. Am. Phys. Soc. **12**, 597 (1967).
[56] G. Scharff-Goldhaber, J. Phys. Soc. Japan, Suppl. **24**, 150 (1968).

observe in Coulomb excitation experiments. Examination of the γ-ray spectra for each of the osmium isotopes reveals some unexplained transitions in the expected energy region from 600 to 900 keV. Because of their low intensity, it has so far proven difficult to positively identify them with the deexcitation of a 0^+ state. Reactions which preferentially populate collective 0^+ levels, such as the (p, t) reactions, would be extremely useful to search for these levels.

E. Quadrupole Moments

Another important test of the Kumar-Baranger calculation rests in the experimental measurements of quadrupole moments of the 2^+, 4^+, and $2^{+\prime}$ levels in the osmium isotopes. The quadrupole moments predicted by these calculations differ significantly from the rotational-model values; the ratio of the values predicted by the two models for all these states varies from approximately 0.9 for Os^{186} to approximately 0.25 for Os^{192}. Recently, a measurement of the quadrupole moment of the 2^+ state in $Os^{190,192}$, employing the reorientation effect in Coulomb excitation by Saladin and coworkers,[42] has yielded results in agreement with the Kumar and Baranger calculations. It is obviously important to extend these measurements to the other excited states, particularly the $2^{+\prime}$ state, in view of the indications from the present measurement that the ratio $|Q_{22}|/|Q_{00}|$ tends to be greater than one in the Os nuclei except for Os^{192}. The latter conclusion is based on the rotational model so that, particularly for $Os^{190,192}$, the result can only be viewed as suggestive. It is interesting to point out that in Er^{166} and Er^{168} this ratio is also reported to be greater than one.[57] In fact, in general, very little is known about the intrinsic quadrupole moments for either the γ or β bands. In most of the phenomenological model calculations, the quadrupole moments for these bands are assumed equal to the ground-state band quadrupole moments.

F. Conclusions

In addition to the above comparisons that were made with the Kumar-Baranger model, it should be noted that this model also quite accurately predicts magnetic moments of the first excited 2^+ states and the ground-state moments of inertia in these nuclei, and reproduces to within ± 50 keV the energies of the 2^+, 4^+, and $2^{+\prime}$ levels.

From all the evidence available to date, the microscopic calculations of Kumar and Baranger have proven to be a useful basis for discussing the structure of the osmium transition region. Considering the nature of the calculations, the agreement with experiment is good except, as has been pointed out in the above text, the model in its present form predicts a more rapid transition from the deformed to the spherical shape than is evident in the experimental data. It would be very instructive to have the calculations further developed by (1) possibly by modifying the relative strengths of the pairing and quadrupole nucleon-nucleon residual forces assumed in the input to the original calculation to favor more the relative strength of the quadrupole force, (2) by the use of more realistic nucleon-nucleon forces, and (3) by extensions of the calculations to include numerical results for other nuclei. In particular, calculations for the mass 150 transition region would be very interesting, since some ambiguities have recently arisen for the neutron 90 nuclei concerning the application of the rotational-model relationships to these nuclei.[58] To complete the evaluation of the original calculations of Kumar and Baranger in the mass 190 region, it is also important to obtain further experimental results on the Pt and W isotopes.

ACKNOWLEDGMENTS

We wish to thank Dr. F. K. McGowan and Dr. W. T. Milner for informing us of their results prior to publication. We also thank Dr. Krishna Kumar and Professor B. R. Mottelson for informative discussions concerning this work. The participation of Dr. I. A. Fraser in some phases of this work is gratefully acknowledged. We would like to express our appreciation to the operating staff of the A. W. Wright Nuclear Structure Laboratory for their assistance in carrying out these measurements.

[57] C. Gunther and D. R. Parsigault, Phys. Rev. **153**, 1297 (1967).

[58] B. R. Mottelson, J. Phys. Soc. Japan, Suppl. **24**, 87 (1968).